

ON THE DEVELOPMENT OF CARBON MATERIALS FOR SPECIFIC APPLICATIONS

B. Viswanathan*, P. Indra Neel and T K Varadarajan

National Centre for Catalysis Research, Department of Chemistry, Indian Institute of Technology, Madras, Chennai – 600036, India

Content:

I. Introduction

II. Carbon Material from Limonea Acidissima Shells for Electrocatalytic Applications

II Carbon Material from Calotropis Gigantea Stems for Catalytic Applications

III. Carbon Materials (as adsorbent) for Adsorptive Desulphurization

IV. Conclusion

IV. Acknowledgements

V. References

I. INTRODUCTION

Materials based on carbon have been evolving all the time. In recent times these materials have given rise to a variety of intriguing possibilities in terms of structure, morphology, texture, properties and applications. However, one of the challenging and desired aspects for carbon materials is to find ways of producing these materials from alternate sources and to tune the textural, structural and surface properties in accordance with the application. The methodologies for generating carbon materials from some of the unusual natural sources like Limonea Acidissima and Calotropis Gigantea are considered. The carbon materials thus obtained have been characterized using a variety of tools. The possibility of modulating the textural properties of these materials has been examined and the appropriate opportunities available have been postulated.

* Corresponding author: Tel.: +91 44 22574241/5245.

Fax: +91 44 22574202/5245.

E-mail address: bvnathan@iitm.ac.in (B. Viswanathan)

The carbon materials synthesized have been exploited for specific applications such as support for noble metals for use in Direct Methanol Fuel Cells and as support for heteropoly acid for the production of gasoline additive. In addition, the utility of some of the activated carbon materials (from commercial sources) for the removal of sulphur from crude petroleum sources is also examined.

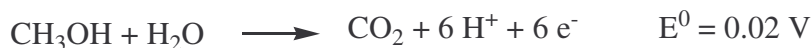
II. CARBON MATERIAL FROM LIMONEA ACIDISSIMA SHELLS FOR ELECTROCATALYTIC APPLICATIONS

Activated carbon materials from natural sources (lignocellulosic materials) have been widely exploited for sorption and catalytic applications. Such materials remained unexplored for energy conversion device applications. Activated carbon material is synthesized from Limonea Acidissima (wood apple) shells using KOH as activating agent. The carbon material (C_{WA} , Carbon from wood apple shell) obtained is used as support for Pt. The electrocatalyst Pt/ C_{WA} is employed for the fabrication of anode for the electrooxidation of MeOH [1]. Issues of insufficient activity and durability of anode electrocatalyst (Pt/ C_{WA}) which are a stumbling blocks in the commercialization of fuel cells were addressed.

1. Fuel Cells as Clean Energy Sources

Fuel cells are efficient and environmentally acceptable energy conversion devices comprising of an electrolyte in contact with an anode (where oxidation of fuel takes place) and a cathode (where reduction of oxygen takes place). In a fuel cell, the chemical energy of the fuel is directly converted to the electrical energy through a chemical reaction [2].

Electric current is generated by the direct electrochemical oxidation of MeOH. The electrooxidation reaction of methanol at the anode can be represented as follows [3]:



The reaction of MeOH electrooxidation bears technological significance in the operation and exploitation of Direct Methanol Fuel Cells. DMFCs hold promise as clean energy source for future transportation demands. Typical stationary and mobile applications of fuel cells include electrification of residences, providing power to mobile phones, lap top computers and other portable electronic devices [4].

2. Challenges in the Development of Fuel Cell Anode Electrocatalysts

Reduction of the expensive Pt metal loading, enhancement of the long term stability of the electrode, improving the CO tolerance of the electrode, reduction of MeOH cross over through the polymer electrolyte membrane, improving the oxygen reduction kinetics, searching for non-noble metal based electrodes and designing of low cost and effective membranes are the typical challenges in the field of DMFC research [5].

Platinum group metals (PGM's) were most widely used for electrode applications. There are two major problems associated with the development of DMFC. The first is poisoning of the electrode by CO [6]. Phosphoric acid fuel cells can withstand upto 2 % CO in the fuel stream. But Proton exchange membrane fuel cells can only withstand ppm levels of CO. The second problem is the high cost restricting the rapid and wide spread commercialization of fuel cells. Reduction in the cost of catalyst is one of the key objectives of fuel cell research. There are two approaches in which one can solve the above two problems. One approach is to find suitable alternative (partial or complete) to the active component i.e., Pt and the second approach is to find suitable alternative to Vulcan XC 72 R carbon black which is the best carbon support material commercially used till date.

To overcome the problem of CO poisoning several attempts, in the direction of designing CO tolerant anode electrocatalysts, have been made. Au, in nano regime, is one of the best known and active catalyst for CO oxidation particularly and interestingly at low temperature. It means alloying Au with Pt can result in a bifunctional catalyst where in Au assists the removal of CO and Pt facilitates with ease and spontaneity the main fuel cell reaction as the poisoned sites (Pt sites where CO is chemisorbed strongly) are regenerated by the presence of Au. Pt has also been alloyed with, oxophilic metals, like Ru, Mo or Sn. Ru acts as a promoter for CO oxidation. The function of Ru was explained in terms of either bifunctional mechanism (Ru promotes CO oxidation of the strongly bound CO on Pt by supplying oxygen source from species like Ru-OH_{ads}) or by the ligand field effect (the energy level of the Pt-Ru alloy catalyst is changed in such a way that the binding strength of CO on Pt site is weakened and correspondingly the oxidation over potential is reduced). Improved CO tolerance facilitates enhancement in activity and durability of the MeOH oxidation electrocatalysts [7]. In addition to

modification to the active component, developments in carbon support too improve the performance of the electrocatalyst for MeOH electrooxidation reaction. Samant et al., [8] in an example generated a catalyst more active than 10 wt.% Pt/Vulcan XC 72 R just by changing the support i.e., by replacing Vulcan XC 72 R with mesoporous carbon produced by sol-gel method.

Even though systems based on PtRu (ternary systems like PtRuOs, PtRuW, PtRuMo and quaternary systems like PtRuSnW or PtRuOsIr) supported on carbon are regarded as the state-of-the art materials for electrocatalysts, improvement is anticipated in the generation of effective and inexpensive electrocatalysts for the electrooxidation of MeOH for practical DMFC applications [9].

3. Anode Electrocatalyst – Role of Carbon Materials

Pt in nanodimensions is the effective catalyst that promotes the adsorption/dissociation of MeOH in acid medium. Some of the approaches to improve Pt utilization, activity and durability of the electrocatalyst include alloying Pt with other transition metals (Ru, Os, W), promoting Pt with metal oxides, optimizing the composition, structure, size and shape of Pt based nanoparticles [10].

Carbon materials are appropriate candidates for supporting Pt. In general, high specific surface area carbon material is employed as support for Pt for fuel cell electrode applications. The carbon support facilitates the dispersion of the stable metal crystallites with favourable electronic and metal support interaction [11]. The carbon support influences the electrochemical properties and in turn the performance of Pt-based electrocatalysts. The nature of carbon material (oxygen surface functional groups, electronic conductivity, pore structure, morphology, electrochemically accessible surface area) determine the electrochemical performance of electrode catalysts. Electronic conductivity, surface area (electro active as well as BET), porosity, micro structure, macro morphology, corrosion resistance and cost are some of the important properties that determine the suitability of a carbon material for electrode applications. Carbon black Vulcan XC-72 R has been the most widely used support material.

Any breakthrough in the commercialization of DMFC's is possible only by significant improvements either in the replacement of *active Pt metal* or *the support carbon material*.

4. Carbon Material from Limonea Ascidiissima Shell by KOH Activation

Limonea Acidissima (Wood Apple) Shells were conceived for the first time as a source for activated carbon. The fruit, Limonia Acidissima, is native to India and other Asian countries. Limonia Acidissima is also called as Feronia Elephantum, Feronia Limonia, Hesperethusa Crenulata, Schinus Limonia, Wood apple, Elephant Apple and Curd fruit. The shells of Limonia Acidissima (wood apple) have features bearing close resemblance to that of coconut shells. Activated carbon from Limonea Acidissima is produced by the chemical activation method using KOH as activating agent.

4.1. Method of Synthesis of Carbon Material



Typical method of synthesis of carbon material involve soaking known amount (50 g) of dried shells of Limonea Acidissima in 100 ml of 50 wt.% KOH solution for 2 h. Excess KOH solution is then decanted. The shells soaked in KOH solution were then dried in air oven at 150 °C

followed by subjecting the same to thermochemical activation in N₂ atmosphere at 800 °C for 2 h. The char thus obtained was subsequently treated with conc. HNO₃. The char to conc. HNO₃ ratio (wt./wt.%) is 1:5.

4.2. Mechanism of KOH Activation

In general the chemical reaction between KOH and carbon material can be written as follows [12]:

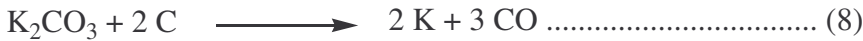
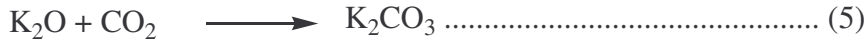
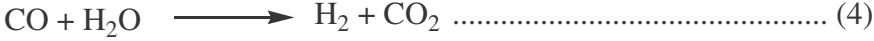
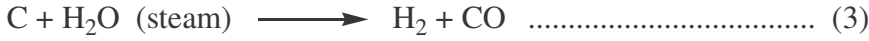


KOH reacts with disordered or amorphous carbon at high temperatures to form K₂CO₃ as well as the decomposition product K₂O along with the evolution of hydrogen.

Considering the decomposition of KOH into K₂O as well as the reducing ability of carbon, additional reactions do take place during the process of activation as shown:

The steam generated in (step 2) causes removal of amorphous carbon as CO as shown in (step 3) leading to formation of pores. Additional carbon is also consumed for reducing K⁺ to K as shown in steps (7) and (8). All these carbon losses contribute to the creation of porous network in the carbon material. It is interesting to note that KOH activation has the benefit of activating the carbon material or the carbon precursor with steam (step 3) as well as activation with K₂CO₃ (step 8). It is to be noted that reaction (8)

is only possible in ungraphitizable carbon materials but not in graphitizable carbon materials possessing structural regularity [13].



In addition to the development of porosity and improvement in specific surface area, another advantage with KOH activation is the generation of surface -OH functional groups. The (-OK) groups formed on the carbon surface upon KOH activation gets transformed to (-OH) groups upon washing with water by ion exchange reaction. Thus in addition to creation of voids by the removal of K, upon washing with water, polar functional groups like -OH are generated making the carbon surface hydrophilic. In fact, producing water soluble (hydrophilic) carbon materials by itself is an important research problem being pursued currently.

4.3. Role of HNO₃ Activation

There are two advantages in treating the char with HNO₃: The advantages are the effective removal of traces of mineral matter in the char, traces of activating agent and its decomposed products and also the generation of oxygen rich surface functional groups [14 – 22].

4.4. Characterization of Carbon Material from Limonea Acidissima

4.4.1. BET sorptometry – Textural properties of Carbon Material

N₂ adsorption – desorption isotherm obtained for the activated carbon from Limonea Acidissima is shown in Fig. 1. The corresponding pore size distribution curve (BJH) is also shown in the insert of Fig. 1.

The isotherm shown in Fig. 1. is of type I characteristic of a microporous material. The pore size distribution indicated that the pore dimensions are lower than 2 nm indicating that the activated carbon material obtained by KOH activation of the shells of Limonea acidissima is micorporous in nature.

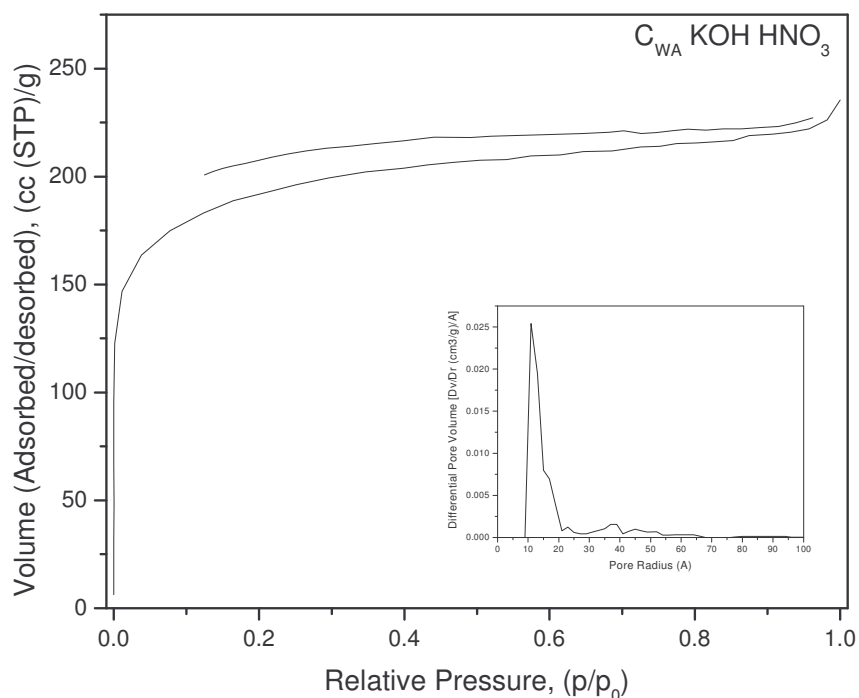


Fig. 1. N_2 adsorption-desorption isotherms of carbon materials prepared from Limonea Acidissima; the corresponding pore size distribution of the activated carbon material is shown in the insert; $S_{BET} = 698 \text{ m}^2/\text{g}$; Pore volume (V_p) = $0.35 \text{ cm}^3/\text{g}$; and Mean pore diameter = 2.0 nm.

4.4.2. XRD Studies - Structural (crystal) details of Carbon Materials

The X-ray diffraction pattern obtained for the activated carbon material from Limonea Acidissima shells is shown in Fig. 2. Two broad diffraction peaks centered around 2θ values of 24° and 43° which are respectively attributed to the reflections from the (002) and (10) planes (the (hk) line is because of intra layer scattering) of carbon material. The values of average crystallite sizes along the c-axis (stacking axis) and the a - axis were determined using Debye – Scherrer equation. The shape factor, k, values of 0.89 and 1.84 were employed for the calculation of values of L_c and L_a values respectively. The diffraction angles as well as the value of full width at half maximum corresponding to the diffraction planes of (002) and (10) were employed for the calculation of values of L_c and L_a values respectively. The values of L_c and L_a were found to be of the order of 1.1 nm and 3.656 nm respectively. The values of L_c and L_a for typical graphitic carbon structure are 0.0670 nm and 0.2461 nm respectively [23, 24].

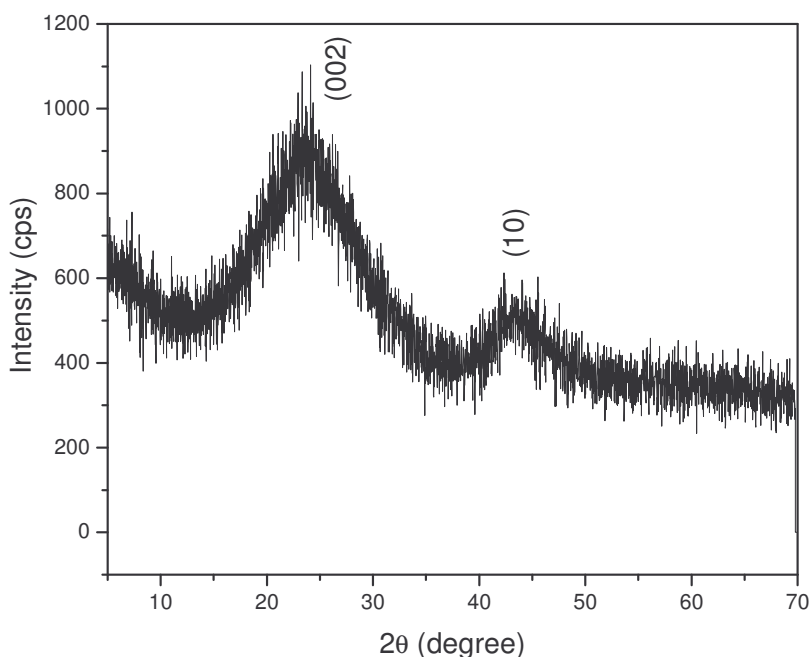


Fig. 2. XRD pattern of carbon material prepared from Limonea Acidissima Shells by KOH activation method

The magnitude of the values of L_c and L_a of the activated carbon materials from Limonea Acidissima (obtained by KOH activation) indicate that the carbon material contained roughly about 16 cell lengths along the c-direction and nearly 15 cell lengths along the a - direction.

4.4.3. Confocal Raman Spectroscopic Studies - Structural (crystal, order, disorder, defect) details of Carbon Materials

Details of structural disorder as well as the crystallographic parameter of the activated carbon material produced by the KOH activation of the shells of Limonia Acidissima were obtained from the Confocal Raman spectrum shown in Fig. 3. Two characteristic Raman peaks centered around 1348 and 1591 cm^{-1} were observed in the confocal Raman spectrum. These two bands were designated as D (disordered) and G (graphitic) bands and were attributed to the A_{1g} and E_{2g} Raman active C-C vibration modes with in the graphitic layer. The Raman peaks at 1348 and 1591 cm^{-1} were called as the first order Raman peaks. Such peaks hold information on the ordering of carbon atoms with in the layer or sheet of carbon but are silent on the way the sheets or layers are stacked one over

other in the c-direction. The other details deduced from Raman spectrum are: $R(I_D/I_G) = 1.408$; $L_a = 4.4/R = 3.125$ nm. This value was compared with the value of L_a deduced from XRD pattern (3.656 nm).

The Raman intensity ratio (the ratio of the integrated intensities of the D and G bands) (I_D/I_G) is a measure of the extent of disorder with in a carbon layer. The R value for the activated carbon material from Limonia Acidissima was found to be 1.408 which is typical of disordered carbon materials like glassy carbon. The average crystallite size along the a - direction, L_a , can also be obtained from the value of Raman Intensity Ratio, R.

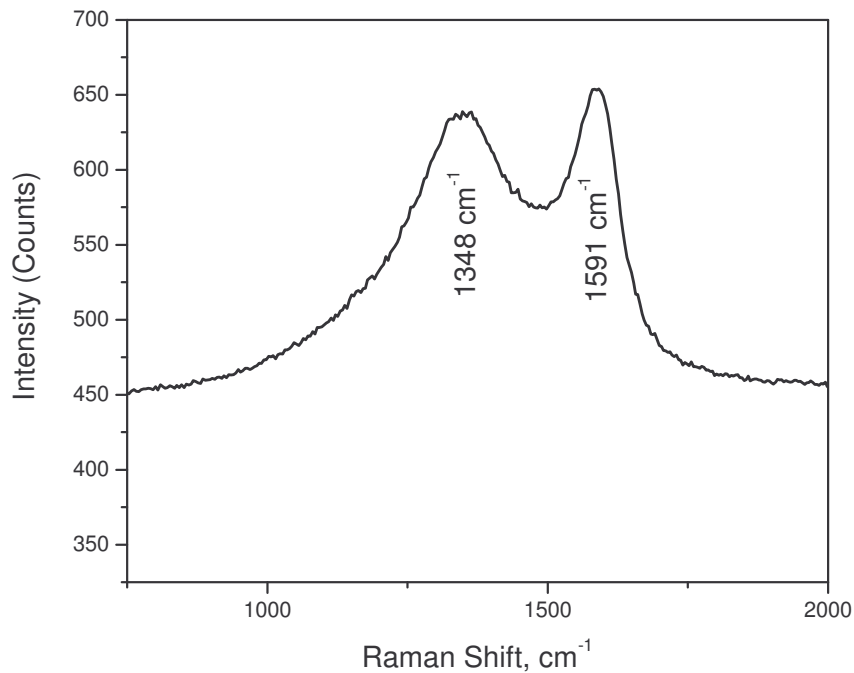


Fig. 3. Confocal Raman spectrum of activated carbon produced from Limonia Acidissima by KOH activation

The L_a value deduced from confocal Raman spectrum, 3.125 nm, is found to be in agreement with that of the L_a value obtained from wide angle X-ray diffraction ($L_a = 3.656$ nm). The slight variation ($\approx 5 \text{ \AA}$) in the L_a value obtained between Confocal Raman spectrum and X-ray diffraction pattern is attributed to the $\pm 7 \%$ error involved in the calculation of the integrated intensity values under the D band G band. Since line width from XRD is more accurately determined compared to the integrated intensity

values under the D and G in the confocal Raman spectrum, the L_a value obtained from wide angle X-ray studies can be reliable.

4.4.4. Electron Paramagnetic Resonance Spectroscopic Studies – Dangling bond concentration

The Electron Paramagnetic Resonance (EPR) spectrum of activated carbon from Limonea Acidissima is shown in Fig. 4. The EPR spectrum was recorded on a X-band EPR spectrometer operating at a microwave frequency of 9.2 GHz at room temperature using diphenyl picryl hydrazyl radical as external reference. The g value of the resonance signal for the activated carbon is 2.03095 which is close to the free electron g – value. The origin of the EPR signal is attributed to the presence of dangling bonds in the carbon structure. The concentration of unpaired spins was found to be 1.3×10^{18} spins/g of the carbon material.

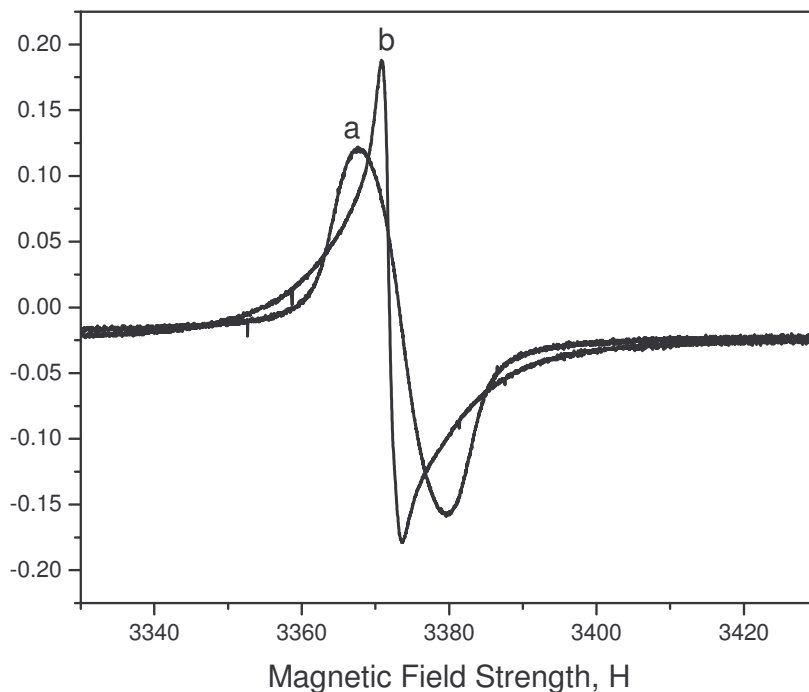


Fig. 4. EPR spectrum of activated carbon from (a) Limonea Acidissima by KOH activation and (b) DPPH (reference)

The spin concentration value of activated carbon from the stems of *Limonea Acidissima* (C_{WA}) is an order of magnitude lower than that of the spin concentration values reported for commercial acetylene (3.8×10^{19}) and graphon (1.1×10^{19}) [25].

The deviation in the spin concentration value in the case of KOH activated sample is because of the saturation of the dangling bonds with potassium, formed during the carbothermal reduction of K_2CO_3 , resulting in the formation of surface C-K bonds which subsequently transform (partially) to C-H bonds upon final treatment with Conc. HNO_3 . Such a transformation is also confirmed from the appearance of C-H bonds in the FT – IR spectrum shown in Fig. 6. The formation of C-K type bonds is also confirmed from the presence of 0.45 wt.% K in the activated carbon material even after treatment with conc. HNO_3 . Manivannan et al., [26] have found the spin concentration values of activated carbon materials, namely, GX203 (from coconut shell precursor), P1400 (from wood precursor) and Med50 (from coconut shell precursor) to be 1.8×10^{17} , 5.8×10^{17} and 1.8×10^{16} spins/g respectively.

4.4.5. Scanning Electron Microscopy and Energy Dispersive X-ray Analysis – Morphology and Elemental Composition

Details of the surface morphology as well as the elemental composition of the activated carbon material were obtained using High resolution scanning electron microscopy (HR SEM, FEL, Model: Quanta 200) equipped with Energy dispersive X-ray analysis facility. Scanning electron microscope images are obtained at a magnification of 4000 x and 10, 000 x and at a scanning voltage of 30 kV.

Highly heterogeneous and rough surface with continuous porous net work is viewed on the surface of the activated carbon produced from *Limonea Acidissima*. The porous network is clearly viewed at higher magnification (10, 000 x) (Fig. 5 (a & b)).

The chemical composition of the activated carbon material is determined using Energy dispersive X-ray analysis. A high carbon content of 74.84 wt.% is derivable from KOH activation of the shells of *Limonea Acidissima*. In spite of treatment with HNO_3 , 0.45 wt.% K is inevitably present in the activated carbon. The oxygen content was found to be 24.7 wt.% (19.83 atomic %).

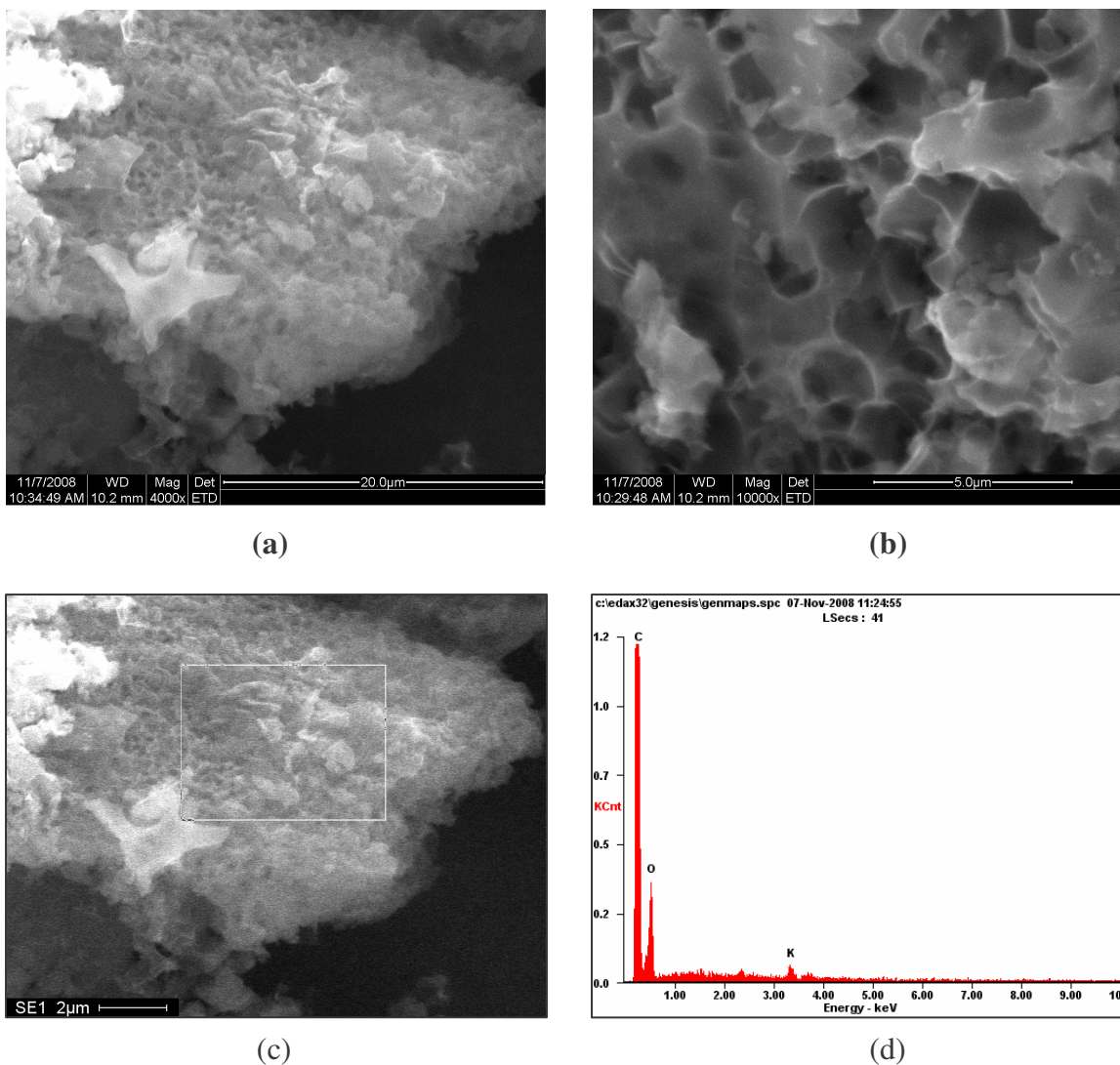


Fig. 5. SEM images and EDAX spectrum from the activated carbon material from *Limonea Acidissima* using KOH activation; at a magnification of (a) 4000 x, (b) 10, 000 x, (c) selected region for elemental analysis and (d) energy dispersive X-ray analysis spectrum

4.4.6. FT – IR spectroscopic Studies – Surface Functional Groups

Fourier transform infrared (FT-IR) spectroscopy provides evidence for the presence of specific functional groups on the surface. The FT – IR spectrum of activated carbon from *Limonea Acidissima*, C_{WA} , was recorded on Shimadzu spectrophotometer. The spectral range of analysis is $450 - 4000 \text{ cm}^{-1}$ with a resolution of 4 cm^{-1} . The spectrum was

obtained in transmission mode at 20 scans. Pressed KBr pellets were prepared by grinding 200 mg of carbon samples with 0.5 g of KBr.

Several characteristic bands were observed in the FT – IR spectrum shown in Fig. 6. and each of the bands has been assigned to specific functional group based on the assignments reported in literature.

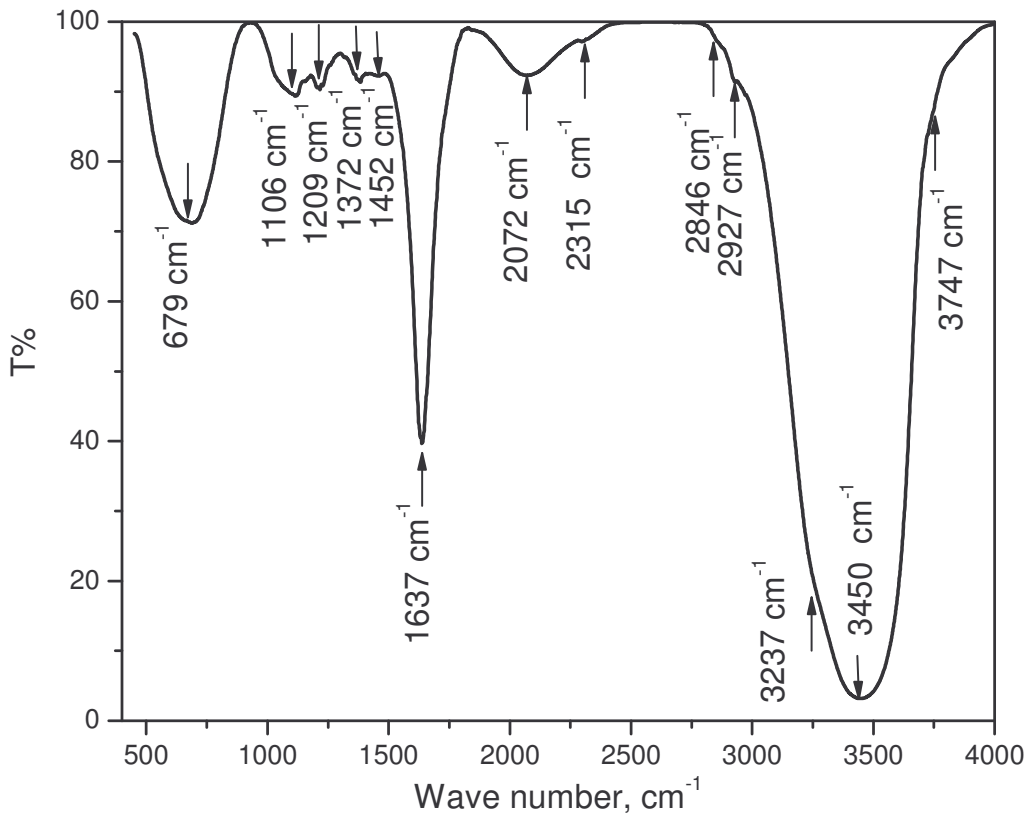


Fig. 6. FT – IR spectrum of activated carbon produced from Limonea Acidissima Shells using KOH activation

Even though a cluster of functional groups are present on the carbon surface, the prominent among them are : a sharp and intense band centered around 1637 cm⁻¹ which is attributed to the carbonyl (C=O) stretching vibration of quinone. The carbon surface is oxidized by treatment with Conc. HNO₃ leading to the generation of such Quinone type carbon functional groups which bear significance in the redox chemistry of carbon materials. Such carbonyl functional groups are known to be pronounced in the case of

oxidized carbon materials rather than the original parent carbon material. In addition, a broad and intense band is observed in the range of 3200 – 3600 cm^{-1} , centered at 3450 cm^{-1} attributable to the O-H stretching vibration of surface hydroxylic groups as well as to the adsorbed waters. The asymmetry of this band (a shoulder at lower wave number, 3237 cm^{-1}) indicate the presence of strong hydrogen bonding interactions.

5. Carbon Material from Limonea Ascidissima Shell for the Fabrication of Anode Electrocatalyst for DMFC Application

Lack of efficient and inexpensive electrocatalyst for MeOH oxidation is a challenge for the large scale utility of direct methanol fuel cells. The objective of the work is to design a cost effective and highly active electrocatalyst by developing new porous carbon material as support for Pt, as alternative to Vulcan XC 72. The developed carbon material exhibited suitable porosity, specific surface area, morphology and surface functionality and resulted in a substantial decrease in the loading of the active component (Pt) by increasing the Pt utilization. In addition the electrocatalyst was found to be tolerant to CO poisoning.

5.1. Preparation of Pt/C catalysts – Impregnation followed by reduction in H_2 atmosphere

Pt supported carbon catalysts have been prepared by impregnating hexachloroplatinic acid in carbon material followed by reduction of Pt^{4+} to Pt(0) in hydrogen atmosphere at 450 °C for 2 h. Catalysts with different wt.% loadings, namely, 5, 10 and 20 wt. %, of active component (Pt) on the carbon support (C_{WA}) were prepared by adding requisite amount of H_2PtCl_6 solution (7.7 mM, 1.0 g $\text{H}_2\text{PtCl}_6 \cdot 6\text{H}_2\text{O}$ dissolved in 250 ml distilled water) to carbon support (C_{WA}). 20 wt. % Pt/Vulcan XC 72 R prepared under identical conditions is employed as reference for comparing the performance of C_{WA} carbon material with that of Vulcan XC 72 R carbon black.

5.1.1. XRD analysis of Pt/C catalysts – Pt Crystallite Size - Presence of Pt in FCC structure

The X-ray diffractograms of 5, 10, and 20 wt.% Pt on carbon material obtained from the shells of Limonea Acidissima (wood apple) are shown in Fig. 7. For comparison the XRD pattern of 20 wt.% Pt/Vulcan XC 72 R is also shown in Fig. 7. Diffraction peaks

characteristic of Pt metal with a face centered cubic lattice are observed and the peaks are all indexed as (111), (200), (220), (311) and (222) (JCPDS file No. 87-0647).

The crystallite size of Pt calculated using Debye-Scherrer equation [27] and the lattice parameter values of Pt metal in the case of each of the catalysts (Pt/C_{WA} and Pt/Vulcan XC 72 R) were calculated. The broad diffraction peak centered around a 2 θ value of 24 corresponds to the (002) reflection of carbon support with a turbostratic graphitic structure. The lattice constant value of \sim 0.39 nm correlated well with the FCC lattice of Pt metal supported on carbon materials [JCPDS file No. 87-0647]. The lattice constant value of pure Pt metal is (0.3923 nm) [28].

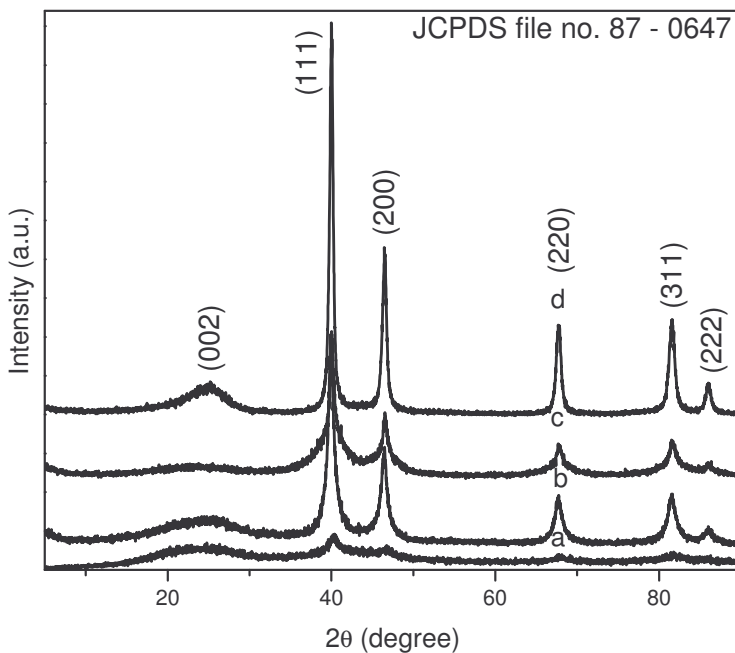


Fig. 7. X-ray diffraction patterns and Pt crystallite sizes of (a) 5 wt.% Pt/C_{WA} (5.0 nm) (b) 10 wt.% Pt/C_{WA} (10.2 nm) (c) 20 wt.% Pt/C_{WA} (10.4 nm) and (d) 20 wt.% Pt/Vulcan XC 72 R (13.1 nm)

The reflection from (220) plane of Pt metal is considered for the calculation of crystallite size as it is away from the region of the broad diffraction peak (from (002) plane) of carbon support. The crystallite size of Pt is found to be dependent on the Pt loading and also on the nature of the carbon support. With the same amount of Pt loading (20 wt.%), the crystallite size of Pt on carbon produced from *Limonea acidissima* shell is

smaller (10.4 nm) than that of the crystallite size of Pt on Vulcan XC 72 R (13.1 nm) indicating better dispersion of Pt on the C_{WA} support due to the enhanced surface oxygen functional groups as well as higher value of specific surface area. Also the Pt crystallite size was found to be the least (5 nm) in the case of 5 wt.% Pt supported on carbon material from Limonea Acidissima indicating better dispersion of Pt particles on the support at lower Pt loadings (5 wt.% Pt). A strong correlation was found between the Pt crystallite size and the wt.% loading of Pt on the carbon support.

5.1.2. BET sorptometric Studies – Textural Properties (specific surface area, total pore volume, mean pore diameter) of Pt/C catalysts

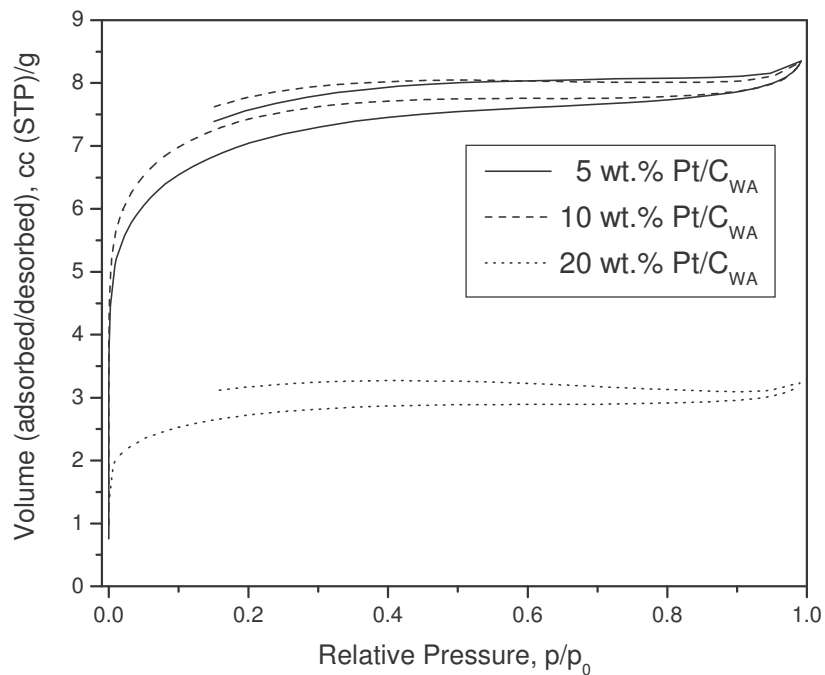


Fig. 8. N_2 adsorption-desorption isotherms of Pt/C_{WA} electro catalysts (a) 5 wt.% Pt/C_{WA}, (b) 10 wt.% Pt/C_{WA} and (c) 20 wt. % Pt/C_{WA}

The textural properties of the Pt/C_{WA} catalysts were investigated by BET sorptometry. The N_2 adsorption-desorption isotherms of carbon (C_{WA}) supported Pt catalysts (5, 10 and 20 wt.%), recorded on a Micromeritics model ASAP2020 porosimeter, are shown in Fig. 8. At all loadings the Pt/C_{WA} catalysts exhibited typical type I isotherms characteristic of microporous solids. This indicates that the pore texture of the support is

retained and no collapse of pore texture has taken place upon impregnating Pt on to the support up to a loading of 20 wt.%.

Another important observation is that the volume of N₂ (adsorbate) adsorbed, decreased drastically as the wt. % loading of Pt increased from 10 wt. % (S_{BET} = 526 m²/g, V_p = 0.288 cm³/g) to 20 wt.% (S_{BET} = 195 m²/g, V_p = 0.115 cm³/g) over C_{WA} support. 10 wt. % Pt/C_{WA} showed similar sorption capacity of the adsorbate as that of 5 wt.% Pt/C_{WA} (S_{BET} = 505 m²/g, V_p = 0.289 cm³/g) even though it is expected to show lower sorption for N₂ compared to 5 wt.% Pt/C_{WA}. In the case of 5 wt. % Pt/C_{WA} catalyst, probably the Pt crystallites (5.0 nm) are finely dispersed over the whole of the carbon support surface. Even though the dispersion of the nanocrystallites of Pt is advantageous, these small crystallites partially block the accessibility of the micropores to the adsorbate (N₂) and this phenomenon is more severe in the case of 5 wt.% Pt/C_{WA}. The non accessibility of the micropores to the adsorbate is also evident from the micro surface area value (deduced from t-plots) of 5 wt.% Pt/C_{WA} (267 m²/g) which is lower than that of the micropore surface area of 10 wt. % Pt./C_{WA} (318 m²/g). Even though no quantitative estimation of the dispersion of Pt over carbon support is made, an appropriate guess can be made about the extent of dispersion from the relative crystallite sizes of Pt in the case of 10 wt.% Pt/C_{WA} (10.2) and 5 wt.% Pt/C_{WA} (5.0 nm). For comparison the textural properties of 20 wt.% Pt/Vulcan XC 72 R catalyst are: (S_{BET} = 123 m²/g, V_p = 0.294 cm³/g).

6. Evaluation of Electrocatalytic Activity of Pt/C Catalysts – Electrooxidation of MeOH

Cyclic voltammetric studies were carried out on a BAS Epsilon potentiast using modified glassy carbon (Bioanalytical system, USA) as the working electrode, Ag/AgCl (saturated KCl) as the reference electrode and a platinum foil (1.5 cm²) as an auxiliary electrode. 0.5 M H₂SO₄ was employed as supporting electrolyte. The electrochemical measurements were carried out in a conventional three-electrode glass cell. The MeOH oxidation reaction was carried out with 1 M CH₃OH in acid medium.

6.1. MeOH Electrooxidation – Significance of Anodic Peaks in the Forward and Reverse Scans

The cyclic voltammograms recorded with electrodes fabricated using 5 wt. %, 10 wt.%, and 20 wt.% Pt supported on carbon material C_{WA} are given in Fig. 9. For comparison the cyclic voltammetric response from the electrode fabricated with 20 wt.% Pt supported Vulcan XC 72 R is also shown in Fig. 9. The feature common to all the cyclic voltammograms is that one anodic peak is observed in the forward scan and in the reverse scan another anodic scan is observed. The anodic peak in the forward scan is attributed to oxidation of MeOH [29, 30, 31, 32, 33, 34]. The anodic peak in the reverse scan is attributed to the removal of the incompletely oxidized carbonaceous species (mostly in the form of linearly bonded Pt=C=O) formed in the forward scan [29].

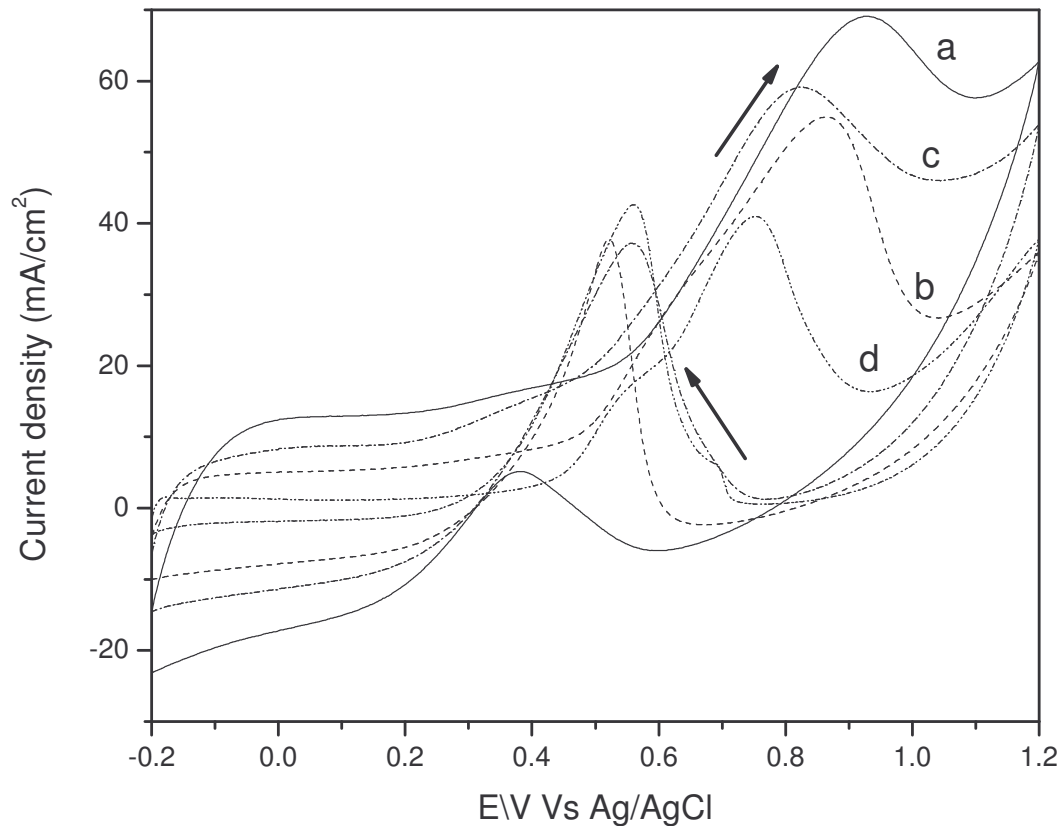


Fig. 9. Cyclic Voltammetric response of (a) GC/ C_{WA} - 5 wt.% Pt - Nafion electrode (b) GC/ C_{WA} - 10 wt.% Pt - Nafion electrode (c) GC/ C_{WA} - 20 wt.% Pt - Nafion electrode and (d) GC/Vulcan XC 72 R - 20 wt.% Pt - Nafion electrode in 0.5 M H_2SO_4 and 1 M MeOH, at a scan rate of 25 mV/sec between -0.2 to 1.2 V Vs Ag/AgCl

6.2. MeOH Electrooxidation – Significance of Onset Potential

The critical parameter that determines the usefulness of an electrode is the onset potential. Less positive value of the onset potential is preferred. Lower onset (less positive potential) potential value implies the requirement of lower energy of the MeOH oxidation reaction to take place [35]. The onset potential value is related to the breaking of the C-H bond of MeOH which is the primary step involved in the mechanism of electrooxidation of MeOH [10]. The onset potential values for the electrooxidation of MeOH deduced from the cyclic voltammograms obtained over different electrode, along with peak potential and current values corresponding to the MeOH oxidation (anodic peak in the forward sweep) as well as the oxidation of intermediate species formed during the oxidation of MeOH (anodic peak in the reverse sweep) are summarized in Table 1. Zhaoling Liu et al., [36] have reported the onset potential values of 0.27 and 0.28 respectively on Pt/Vulcan XC 72 R and Pt/CNT's for the electrooxidation of MeOH in 1 M H₂SO₄ and 2 M MeOH at a scan rate of 50 mV/sec

Table 1. Effect of Pt loading (5, 10 and 20 wt.%) as well as the nature of carbon support (C_{WA} and Vulcan XC 72 R) on the electro catalytic activity of MeOH Electrooxidation - Comparison of electrocatalytic activity of Pt/C_{WA} and Pt/Vulcan XC 72 R

S. No.	Electrode	Onset Potential, V	i_f/i_b	Activity*			
				Forward sweep		Reverse sweep	
				I (mA/cm ²)	E (V)	I (mA/cm ²)	E (V)
1	GC/C _{WA} -5 % Pt-Nafion	0.21	14.4	69.0	0.92	4.97	0.37
2	GC/C _{WA} -10 % Pt-Nafion	0.18	1.45	55.0	0.86	37.6	0.52
3	GC/C _{WA} -20 % Pt-Nafion	0.18	1.60	58.9	0.82	37.28	0.51
4	GC/Vulcan XC 72 R-20 % Pt-Nafion	0.25	0.96	40.9	0.75	42.6	0.56

*Activity evaluated 0.5 M H₂SO₄ and 1 M MeOH, at a scan rate of 25 mV/sec between -0.2 to 1.2 V Vs Ag/AgCl

The onset potential being little lower (0.21 V) than the commercial vulcan carbon (0.25 V), 5 wt.% Pt/C_{WA}, catalyst showed higher current density which is an indication of higher electrochemical catalytic activity. Such a high current values derivable from the modest wt.% loadings of Pt is an indication of the effective utilization of Pt over the C_{WA} support. The improved performance of the electrocatalyst, 5 wt.% Pt/C_{WA}, is attributed to the high electro catalytic activity of the Pt nano crystallites (5.0 nm) finely dispersed over the carbon support. The fine dispersion is facilitated by the lower amount of Pt loading, high specific surface area of the support as well as the hydrophilic (oxophilic) quinone surface functional groups present on the carbon support surface.

6.3. MeOH Electrooxidation – Significance of the Ratio of Anodic Peak Current Densities in the Forward and Reverse Scans, (i_f/i_b)

The ratio of the anodic peak current densities in the forward (i_f) and reverse (i_b) scans too gives a measure of the catalytic performance. A higher i_f/i_b ratio indicates superior oxidation activity of methanol during the anodic scan and less accumulation of carbonaceous species on the nanocatalyst surface and thus an indication of better CO tolerance. The i_f/i_b value in the case of 5 wt.% Pt/C_{WA} catalyst is 14.4 which is an order of magnitude higher than that of either 20 wt.% Pt/C_{WA} or 20 wt.% Pt/Vulcan XC 72. The i_f/i_b value of the electrocatalyst produced from commercial fuel cell grade Vulcan XC 72 carbon was found to be 0.96. At all the loadings of Pt, the electrodes fabricated using C_{WA} carbon materials showed an i_f/i_b value greater than 0.96 (value obtained for Vulcan XC 72 R based catalyst). For comparison, the i_f/i_b value for 20 wt.% PtRu/C catalyst of commercial Johnson Matthey sample is 1.33 [37]. Zhibin Lei et al., [38] have observed the i_f/i_b values of 2.22, 1.47, 1.33, and 1.11 on 20 wt.% Pt supported on nitrogen containing ordered mesoporous carbon heat treated at 600, 700, 850 and 900 °C. The afore mentioned catalysts were prepared by wet chemical reduction method. For comparison, Zhibin Lei et al., [38] have evaluated the performance of 20 wt. % Pt/Vulcan XC 72 under identical conditions and observed an i_f/i_b value of 0.89. The aforementioned value is close to the value shown in Table 1.

6.4. MeOH Electrooxidation – Effect of Scan Rate

The effect of scan rate on the electrochemical performance (current out put) of different electrodes, namely, 5, 10 and 20 wt. % Pt/C_{WA}/GC at the scan rates of 5, 10, 15, 20 and

25 mV/sec in 0.5 M H₂SO₄ and 1 M MeOH between – 0.2 to 1.2 V Vs Ag/AgCl is evaluated. For comparison the current response to variation in scan rate for the electrode fabricated using Vulcan XC 72 R as support with 20 wt.% Pt loading was also studied. It was observed that the peak current density values due to the MeOH oxidation increased as the scan rate increased from 5 to 25 mV/sec irrespective of the nature (amount of active compound or the type of carbon support) of the catalyst. A small increment in the peak potential with an increase in the scan rate is also observed.

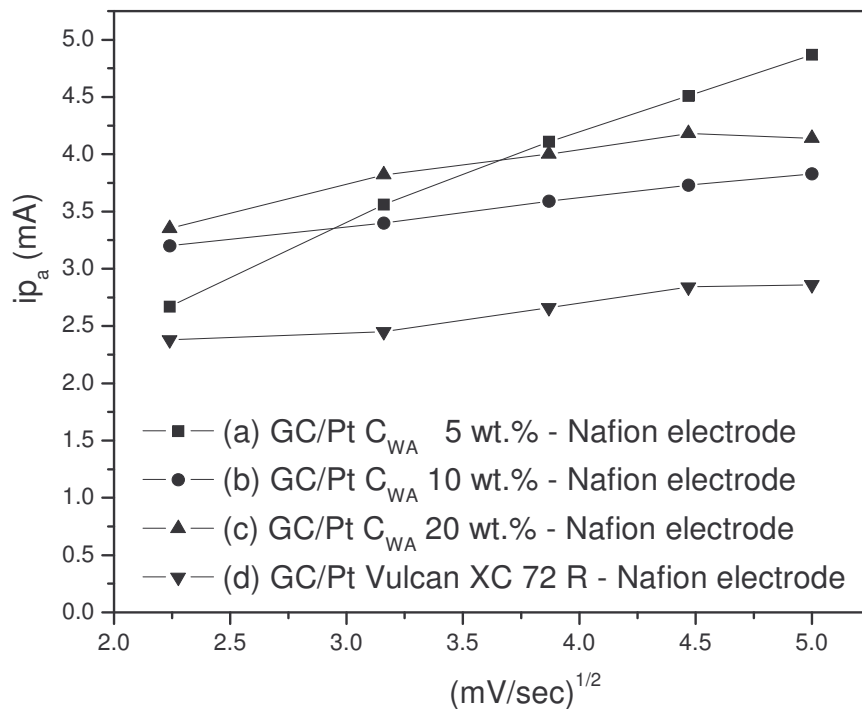


Fig. 10. Dependence of peak currents on the square roots of scan rates for (a) GC/Pt C_{WA} 5 wt.%- Nafion electrode, (b) GC/Pt C_{WA} 10 wt.%- Nafion electrode, (c) GC/Pt C_{WA} 20 wt.%- Nafion electrode and (d) GC/Pt Vulcan XC 72 20 wt.% - Nafion electrode in 0.5 M H₂SO₄ and 1 M MeOH, at different scan rates (5, 10, 15, 20 and 25 mV/sec) between -0.2 to 1.2 V Vs Ag/AgCl

The peak currents were found to be linearly proportional to the square root of scan rates as shown in Fig. 10. in all the cases. Such a linear proportionality relationship between

the current response and square root of scan rate indicate that the electrooxidation process of MeOH is controlled by diffusion [39, 40].

6.5. MeOH Electrooxidation – Evaluation of Stability of the Electrode - Chronoamperometry

The long term stability of the fabricated electrodes was evaluated by chronoamperometric studies carried out for a duration of 3 h with the electrode being polarized at + 0.6 V Vs Ag/AgCl in 0.5 M H₂SO₄ and 1 M MeOH. The current density Vs time plots derived from the electrodes based on 5, 10 and 20 wt.% Pt/C_{WA} are shown in Fig. 11. The initial and final (after 3 h duration) current density values derivable from the electrodes fabricated from 5, 10 and 20 wt. % Pt/C_{WA} electrocatalysts were summarized in Table 2. The percentage decrease of the activity of the afore mentioned electrodes after 3 h is also shown in Table 2.

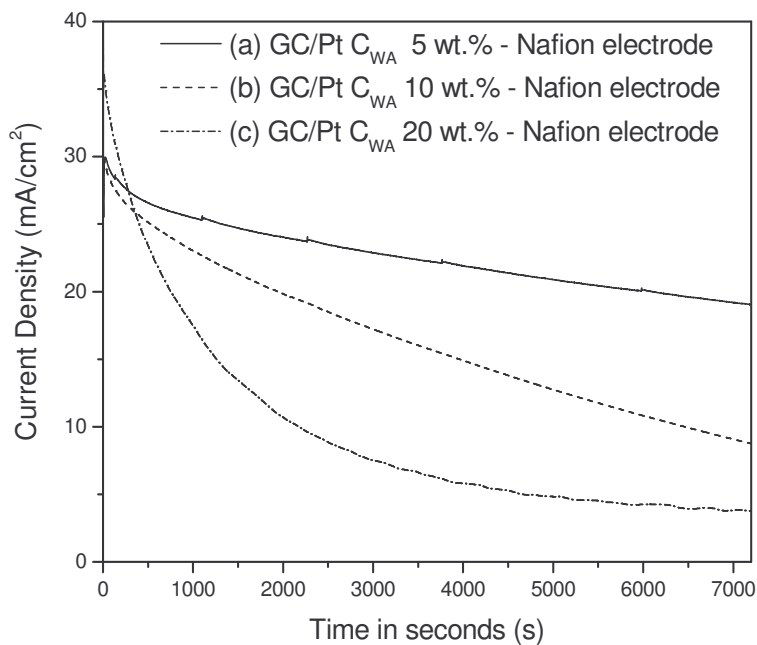


Fig. 11. Chronoamperometric response of (a) GC/C_{WA} - 5 wt.% Pt - Nafion electrode (b) GC/C_{WA} - 10 wt.% Pt - Nafion electrode and (c) GC/C_{WA} - 20 wt.% Pt – Nafion electrode polarized at + 0.6 V Vs Ag/AgCl in 0.5 M H₂SO₄/ 1 M MeOH for 3 hours

Among the electrodes studied, the 20 wt. % Pt/C_{WA} catalyst based electrode showed least stability with a 89 percentage decrease of initial activity at the end of 3h. Such a poor performance is the result of the higher crystallite size (10.4 nm) of Pt formed in the case of 20 wt.% Pt/C_{WA} catalyst. In sharp contrast, as expected, the electrode fabricated using 5 wt.% Pt/C_{WA} possessing the smallest Pt crystallites (5.0 nm) as well as high i_f/i_b ratio showed highest stability. Only 24 % loss in the initial activity is observed even at the end of 3 h in the case of the GC/C_{WA} – 5% Pt – Nafion electrode. Thus it is clear that the stability of the electrode is based on the smaller crystallite size of Pt as well as the high CO tolerance (high i_f/i_b ratio value).

Table 2. Evaluation of the stability of C_{WA} based electrodes for the electrooxidation of MeOH in half cell mode

S. No.	Electrode	Activity*		% Decrease in activity after 3 h at + 0.6 V
		Initial (I), mAcm ⁻²	Final (I), mAcm ⁻²	
1	GC/C _{WA} -5 % Pt-Nafion	25.2	19.1	24
2	GC/C _{WA} -10 % Pt-Nafion	29.7	19.0	36
3	GC/C _{WA} -20 % Pt-Nafion	36.1	3.7	89

*Activity evaluated in 0.5 M H₂SO₄ and 1 M CH₃OH for 3 h with the electrode being polarized at + 0.6 V Vs Ag/AgCl

The activated carbon material produced from Limonea Acidissima by KOH activation is a promising support for Pt for the electrooxidation of MeOH. The excellent performance of 5 wt. % Pt/C_{WA} is attributed to the increase in the extent of utilization of Pt metal. Thus the use of carbon material from Limonea acidissima as support for Pt offered the promise of effective utilization of Pt, high electrooxidation (MeOH) activity, high CO tolerance and long term stability. A strong correlation was found between the Pt crystallite size and the electrooxidation activity and stability of the carbon supported Pt catalysts.

III CARBON MATERIAL FROM CALOTROPIS GIGANTEA STEMS FOR CATALYTIC APPLICATIONS

Industrially, activated carbon materials are produced from either coal or lignocellulosic materials [41]. In addition to several specific advantages like retention of the structural features of the original plant tissue (biotemplating feature), carbon materials produced from botanical sources possess high carbon content. The O/C and H/C ratio's are lower in the case of carbon materials produced from plant sources. Char from botanical sources or the raw plant material lose H and O more easily than C when heat treated in inert environment [42]. Thus the carbonization yield is large for lignocellulosic materials.

High surface area, microporous activated carbon with a narrow pore size distribution from the dried stems of *Calotropis Gigantea* [43]. *Calotropis Gigantea* is a waste land weed native of India. Transformation of a unwanted material into a value added product (activated carbon) is an important strategy not only to generate new materials but also to control pollution.

1. Synthesis of Carbon Materials from *Calotropis Gigantea* Stems using Transition Metal Salt as Activating Agent

1.1. Use of $ZnCl_2$ as Activating Agent

Adsorption properties of carbon materials are enhanced upon chemical activation [44]. In general, the chemical species used for activation are normally dehydrating agents. They influence the pyrolytic decomposition of carbon precursor. $ZnCl_2$ is extensively used as activating agent in the synthesis of activated carbon materials [44 - 56].

1.2. Role of $ZnCl_2$ in the Chemical Activation

The ability of $ZnCl_2$ to activate (generate porosity) in carbon precursors is based on its dehydrating function. During the process of activation, $ZnCl_2$ eliminates hydrogen and oxygen atoms of carbon materials as water rather than as oxygenated organic compounds leading to the generation of porosity as well as enhancing the carbon content [44].

1.3. Method of Synthesis of Activated Carbon using $ZnCl_2$ as Activating Agent

Activated carbon material is produced from *Calotropis Gigantea* stems using $ZnCl_2$ as activating agent. Char (as synthesized) from *Calotropis Gigantea* is produced by heating the dried stems of the plant in muffle furnace at 300 °C [43].



The coal obtained is ground, sieved and treated with Conc. HCl to remove alkali and alkaline metal impurities. The char is further treated with base (NaOH) remove silica which is inherently present. The process of activation with ZnCl₂ is carried out at 800 °C in N₂ atmosphere for 8 h with varying amounts of activating agent to char (wt./wt. %) ratios, namely, 1, 2, 3, 4 and 5. ZnCl₂ is added to the char in solid state by mechanical grinding.

1.4. Characterization of Activated Carbon Produced from ZnCl₂ Activation

Textural and structural parameters and properties of the activated carbon materials were found to be influenced by the amount of the activating agent (ZnCl₂) as revealed from the Sorptometric, XRD and Confocal Raman studies.

1.4.1. BET sorptometry – Textural Properties

Irrespective of the amount of the activating agent, all the activated carbon materials presented type I adsorption isotherms for N₂ adsorption at 77 K typical of microporous materials. The specific surface area values, total pore volume as well as the average pore diameter details deduced from the isotherms are summarized in Table 3.

Table 3. Effect of amount of activating agent (ZnCl₂) on the textural properties of carbon materials produced from Calotropis Gigantea

S. No.	Sample	ZnCl ₂ : C (wt./wt.%)	S _{BET} (m ² /g)	V _P (cm ³ /g)	Mean Pore Diameter ⁱⁱ (nm)
1	Char	0	97	0.08	3.3
2	ⁱ AC1	1	356	0.21	2.36
3	AC2	2	493	0.25	2.03
4	AC3	3	564	0.30	2.13
5	AC4	4	573	0.29	2.02
6	AC5	5	553	0.29	2.1

i. AC – Activated carbon

ii. Mean Pore Diameter, $d = 4V/A$ (in nm)

where V is the total pore volume and A is the specific surface area

The specific surface area values of the carbon materials produced gradually increased with an increase in the ZnCl₂ to char (wt./wt.%) ratio of 4 and beyond which no increase in the S_{BET} value is observed indicating that the optimum value of ZnCl₂:Char ratio is 4.

1.4.2. XRD Studies – Crystallographic Structure

Crystallographic parameters of the activated carbon materials produced by ZnCl₂ activation of Calotropis Gigantea were obtained from X-ray diffraction studies.

Three typical broad diffraction peaks centered around 2θ values of 25, 44 and 80° are visible in the activated carbons generated with the activating agent to char impregnation ratios of 1, 2, 3, 4 and 5. The two broad peaks centered around the 2θ values of 25 and 44 are attributed (002) and (10) diffraction peaks of turbostratic carbon structure [57]. The origin of the broad peak around 2θ value of 80° is not yet clearly known. The (001) line is because of interlayer scattering where as the (hk) line is because of intra layer scattering. Thus the extent of graphitization is revealed by the appearance of general (hkl) reflections [58, 59, 60]. The occurrence of broad diffraction bands centered around 2θ values of 25 and 44 indicate better layer alignment as well as an increased regularity in crystal structure [61].

Table 4. Effect of amount of activating agent (ZnCl₂) on the structural properties of carbon materials produced from Calotropis Gigantea

S. No.	Sample	ZnCl ₂ : C (wt./wt.%)	d ₀₀₂ (nm)	L _c (nm)	L _a (nm)
1	¹ AC1	1	0.356	1.04	3.94
2	AC2	2	0.356	1.02	3.50
3	AC3	3	0.353	1.03	3.96
4	AC4	4	0.356	0.91	3.72
5	AC5	5	0.350	0.94	3.80

i. AC – Activated carbon

The interlayer spacing values, d₀₀₂, and the crystallite size values along the c (L_c) and a (L_a) axis of the turbostratic graphitic carbon were deduced from the X-ray diffractograms

are summarized in Table 4. Using Scherrer equation (shown below), the crystallite size along the c-axis, L_c and the size of the large planes, L_a , were determined from the full width at half maximum of the diffraction peaks centered at 2θ values of 25 and 44 which were respectively indexed to the (002) and (10) diffraction planes of carbon structure.

The interlayer spacing values, d_{002} , almost remained unchanged with impregnation ratio of $ZnCl_2$ to char. The interlayer spacing values, d_{002} , summarized in Table 4 are in the range of 0.35 to 0.356 nm. The afore mentioned values were greater than 0.335 nm, which is the typical value of the interlayer spacing for pure graphitic carbon. L_c values for different activated carbon materials, summarized in Table 4, are of the order of 1 nm. A decreasing trend in the L_c value is observed with an increase in the amount of the activating agent. The L_c value is the smallest for the activated carbon with the highest S_{BET} value. The L_a values varied in the range of 3.5 to 3.96 nm. For typical graphitic carbon, the L_c and L_a values are respectively 0.06708 nm and 0.2461 nm. The magnitude of L_c and L_a values of the activated carbon materials from *Calotropis Gigantea* (obtained by $ZnCl_2$ activation) indicate that the carbon material contained roughly about 2 cell length along the c-direction and about 14 – 16 cell lengths along the a - direction.

1.4.3. Raman Scattering Studies – Order and Disorder in Carbon Structure

Important information pertaining to the disordered (defect) and ordered complex micro structure of carbon materials is obtained from Raman scattering studies [26, 58, 62 – 73]

The microstructural changes and the extent of crystallographic disorder (concentration of lattice defects in the graphitic structure) in the activated carbon materials produced from *Calotropis Gigantia* by employing $ZnCl_2$ as activating agent were analysed using confocal Raman Spectroscopic studies. The Raman spectra, shown in Fig. 12, resulting from activated carbon materials produced with varying the ratios of the activating agent ($ZnCl_2$) to the char (wt./wt.%), namely, 1, 2, 3, 4 and 5, were recorded on Confocal Raman instrument (CRM 200) using Ar ion laser (514.5 nm) as irradiation source.

Irrespective of the amount of the activating agent, all the carbon materials, showed two first order Raman lines. Those lines that appear in the energy region of 1200 – 1600 cm^{-1} are termed as first order Raman lines. On the contrary the Raman lines that appear in higher energy region, typically in the range of 2400 – 3300 cm^{-1} are termed as second

order Raman lines. The information derived from the features of first order Raman lines is different from the information deduced from the feature of the second order Raman lines and both of them are important to access the structure order or disorder in the carbon structure whether it be amorphous or graphitic. First order Raman lines speak only about the structural order or disorder with in the carbon sheet or layer, ie, carbon plane along a-axis. First order Raman lines are silent about the stacking order or disorder in carbon structure. On the contrary, second order lines hold information about the structural (stracking) disorder along the crystallographic c-axis [74].

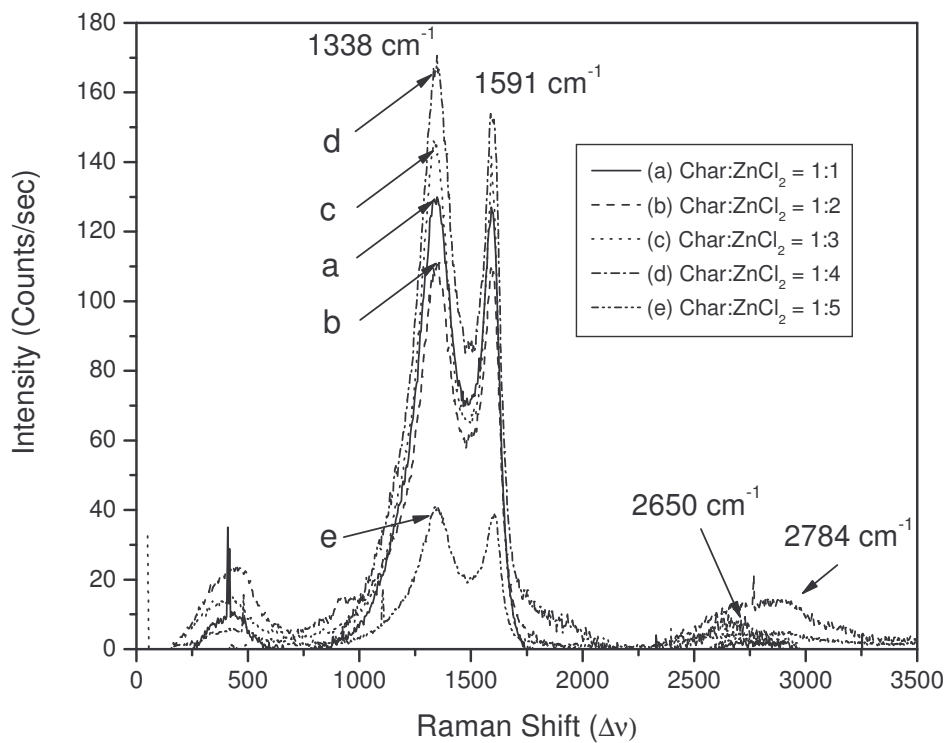


Fig. 12. Confocal Raman spectra of activated carbon materials prepared from *Calotropis Gigantea* with a Char to ZnCl_2 ratio (wt./wt.%) of (a) 1:1, (b) 1:2, (c) 1:3, (d) 1:4 and (e) 1:5

The two first order lines centered around 1590 and 1348 cm^{-1} are attributed to the graphitic and disordered carbon structure. Here the term “graphitic” means carbon atoms which are three coordinated and are bound by sp^2 type bonding orbitals. The term “graphitic” has nothing to do with the stacking of layers along c - direction. The disorder

in the carbon sheet may be because of the non-planar microstructure distortions or because of the disorganized regions near the crystal edges. Lattice defects such as edge dislocation and lattice vacancies too contribute to the band at 1348 cm^{-1} .

In general the band around 1348 cm^{-1} attributable to disordered carbon structure with in the carbon sheet is termed as D band and the Raman signal around 1580 cm^{-1} attributable to the graphitic ordering (with in the layer of carbon) is designated as G band. The G band is because of the E_{2g} Raman active mode arising from the C-C stretching where as the D band results from the A_{1g} Raman mode. Important information extracted from the Raman spectra in Fig. 12. is summarized in Table 5.

Table 5. Structural parameters of the activated carbon materials from Calotropis Gignatea activated with ZnCl_2 deduced from Raman Spectra

S. No.	Sample	$\text{ZnCl}_2 : \text{C}$ (wt./wt.%)	Peak Intensity Frequency, ν_x, cm^{-1}		$R = I_D/I_G$	L_a (nm) = $4.4/R$ (From Raman)	L_a (nm) (from XRD)
			G band	D band			
1	¹ AC1	1	1591	1348	1.40	3.14	3.94
2	AC2	2	1591	1355	1.42	3.09	3.50
3	AC3	3	1591	1331	1.33	3.30	3.96
4	AC4	4	1587	1348	1.48	2.97	3.72
5	AC5	5	1606	1348	1.53	2.87	3.80

The Raman intensity ratio which is a measure of the extent of disorder (quantity of defects and vacancies and dislocations) is found to decrease initially upto the activating agent to char impregnation ratio of 3 beyond which the R value increased. The disorder induced into the carbon structure is increased beyond a ZnCl_2 to char (wt./wt.%) ratio of 3. An inverse proportionality relation is observed between the value of R and the stack width L_a (crystallite size along a-axis). The position of the D band (peak intensity position) as well as the relative intensity of D band were found to be structure sensitive. An increase in the frequency value of the D band was correlated to the decrease in the crystallite size (L_a) and vice versa. A strong correlation between the structural parameters

deduced from XRD studies (Table 4) as well as Raman studies (Table 5) was observed as the two afore mentioned techniques are mutually complimentary to each other. Interestingly, the L_a values ($L_a = 44/R$ in \AA) deduced from the relative intensity of the D band of the activated carbon materials correlated well with the L_a values obtained from XRD studies using Scherrer equation (Table 4). This emphasizes that XRD and Raman studies are equally informative on the crystallographic disorder in carbon structure. But it should be noted that the measurement of line width from the XRD is more accurate than the measurement of the integrated peak intensity values deduced from the Raman spectra. As a result the L_a values derived from XRD are more reliable than those deduced from Raman spectra. In addition, the integrated intensity values from Raman spectra are sensitive to the choice of the base line. As a result, the Raman intensity ratio's (R) shown in Table 5 are uncertain upto $\pm 7\%$.

1.4.4. Scanning Electron Microscopic Analysis – Details of Surface Morphology

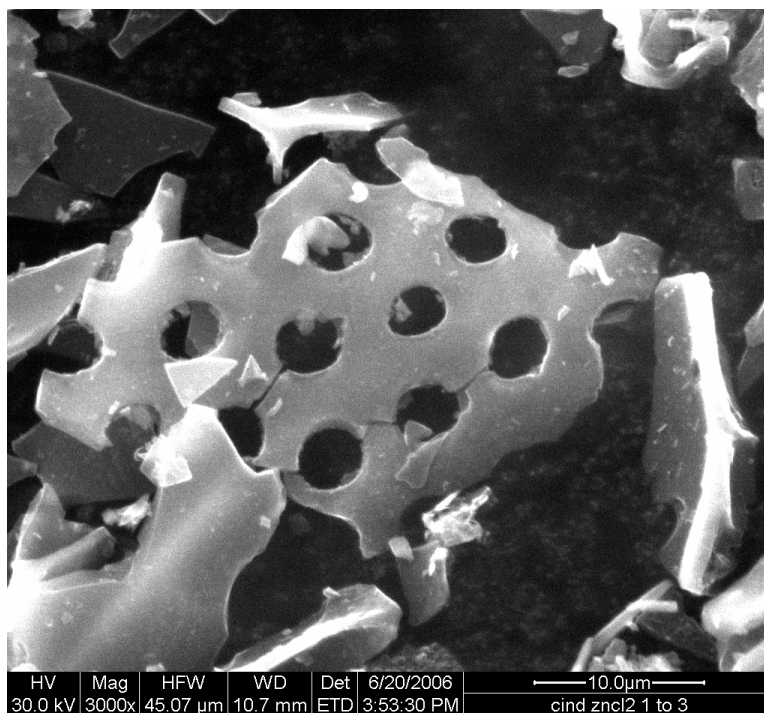


Fig. 13. SEM image of Activated Carbon from Calotropis Gigantia activated with ZnCl_2 (wt/wt. % ratio of Char: ZnCl_2 is 1:3) (reproduced from ref. 43)

Well aligned uniform cylindrical pores of diameter (size) 2.4 μm are observed on the carbon surface as shown in Fig. 13. The maximum values of specific surface area and pore volume values from ZnCl_2 activation of the stems of *Calotropis Gigantea* are only 573 m^2/g and 0.29 cc/g . To attain further improvements in the textural parameters, the usefulness of alkali metal carbonates as chemical activating agents is examined.

2. Synthesis of Carbon Materials from *Calotropis Gigantea* Stems using Alkali Metal Carbonates as Activating Agent

The effect of alkali metal carbonate (Li_2CO_3 , Na_2CO_3 and K_2CO_3) activation on the microstructural, textural and chemical properties of activated carbon is evaluated. The char was obtained by heating a known amount of dried stems of plant in a muffle furnace at 300 $^\circ\text{C}$ for 30 min as a result of which volatile matter is eliminated resulting in a carbon rich material. The char thus obtained was ground and sieved through a 200 mesh sieve to obtain fine carbon particles.

2.1. Characterization of Carbon Materials produced using Alkali Metal Carbonates as Activating Agent

2.1.1. ^{13}C MAS NMR – Chemical Structure of Carbon Material

Useful information on the chemical changes in the original lignocellulosic composition during the initial stages of pyrolysis can be obtained from ^{13}C MAS NMR spectroscopic studies. The ^{13}C nuclei belonging to the aromatic carbons resonate at a frequency range distinctly different from that of the aliphatic carbon making NMR an indispensable tool for the analysis of structural details of the carbon materials. Thus valuable information on the chemical environment of carbon nuclei in condensed aromatic systems can be obtained from NMR spectra.

The ^{13}C MAS NMR spectrum of the char from *Calotropis Gigantea* was recorded on Bruker Avance 400 spectrometer operating at 100.6 MHz (Magnetic field = 9.4 T). The experiments were carried out using silicon nitride rotors spinning at a frequency of about 5.0 to 6.0 kHz. About 1000 transients were recorded. The chemical shifts were externally referenced to tetramethyl silane (TMS). Adamantane was used for setting the reference frequency. The evolution of highly aromatic structure from the pyrolysis of original lignocellulosic material (plant stems) is discernable from the high resolution ^{13}C MAS NMR spectrum of the char shown in Fig. 14. The strong resonance line near 121 ppm

from TMS is characteristic of carbon nuclei in the aromatic planes. In addition, two more broad resonance signals at 35 and 200 ppm attributable, respectively, to aliphatic chains of polymethylene type and ketonic carbon groups were observed in the ^{13}C MAS NMR spectrum of the char.

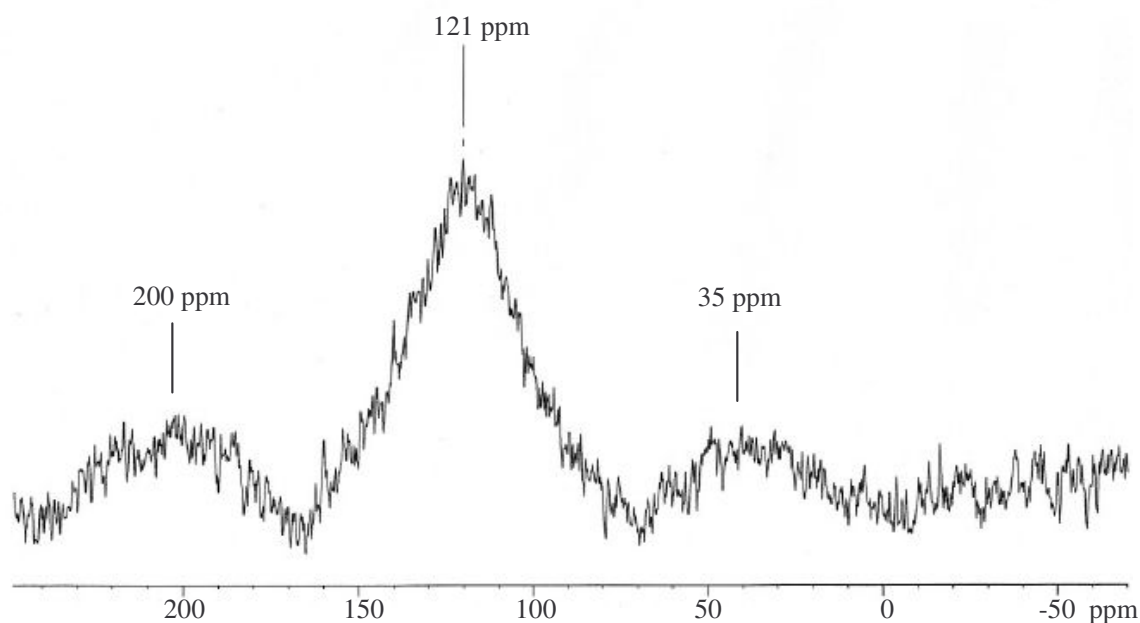


Fig. 14. ^{13}C MAS NMR spectrum of the char (as synthesized) from *Calotropis Gigantea* [reproduced from ref. 43]

In general, the three main structural components of stems of plant like *Calotropis Gigantea* are hemicellulose, cellulose and lignin. Among several structural components of the plant, hemicelluloses are more sensitive to temperature and they are the first to decompose in the temperature range of 200 to 260 °C during pyrolysis. Cellulose is thermally more stable than hemicellulose and will decompose in the range of 240 – 400 °C releasing structural water. In addition rupture of the glycosidic linkages also takes place. Aromatization takes place subsequently. Lignin is the most thermally stable component. Decomposition of lignin takes place in the temperature range of 280 – 550 °C resulting in the formation of large amount of aromatics. Typical structural building units of Cellulose and Lignin (guaiacyl unit) are shown below in Fig. 15.

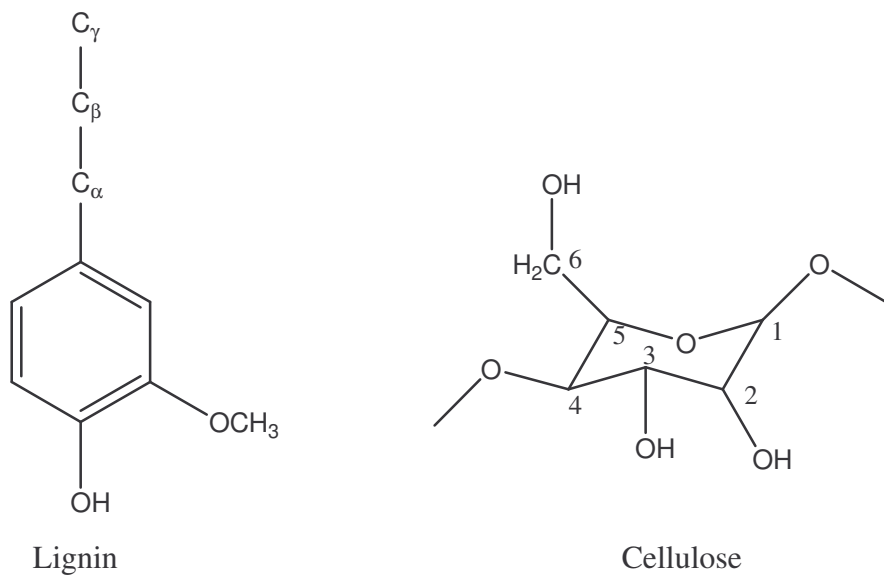


Fig. 15. Typical structural building units of Lignin and Cellulose

Typically, for lignin, a resonance line at 56.8 ppm associated with methoxy groups and also another resonance line between 115 and 150 ppm attributable to aromatic carbons are observed. The carbon nuclei from Cellulose structure resonate at the following chemical shift values: C-1 at 105.8 ppm, C-2, 3, 5 at 73.2 and 75.5 ppm, C-4 at 84.4 and 89.3 ppm and C-6 at 63.5 and 65.0 ppm. The carbon nuclei characteristic of hemicellulose structure results in two resonance signals at chemical shift values of 21.8 and 174 ppm respectively corresponding to the methyl and carbonyl carbon nuclei.

Thus the absence of resonance signals characteristic of cellulosic and hemicellulosic structure in the ¹³C MAS NMR spectrum of the char produced from *Calotropis Gigantea* (Fig. 14) indicating the break down of carbohydrate structure (cellulose and hemicellulose) as a result of pyrolysis and also the conversion of aliphatic groups into aromatic system. The broad and strong resonance signal observed at 121 ppm corresponding to condensed aromatic system with a turbostratic graphitic structure is a contribution from the complete thermal decomposition of carbohydrate (cellulose and hemicellulose) structure and partial decomposition of lignin structure and also the subsequent reorientation of carbon containing short lived radical intermediates to hexagonal layered structure of aromatic carbon. The undecomposed component of lignin

also contributes to the intensity of the signal at 121 ppm. Infact, chars were supposed to comprise of interwoven network of carbon “ribbons” containing hexagonally arrayed carbon layers – a turbostratic.

The char obtained is subjected to activation with varying amounts of K_2CO_3 . The K_2CO_3 to char (wt./wt.%) ratio was varied from 1, 2, 3, 4 and 5 in N_2 at a temperature of 800 °C for 8 h. The material started to burn with glowing when removed from furnace confirming the formation of metallic K by the reduction of K_2CO_3 by C. In air or O_2 at 1 atm, the alkali metals are known to burn [81]. The material is ground instantaneously and treated with Conc. HCl to remove the metallic compounds. The resulting material is filtered and washed with excess distilled water to remove traces of chloride.

^{13}C NMR spectra for the activated carbon samples, obtained by K_2CO_3 activation at 800 °C, could not be recorded because of the problem with the tuning process. Such a problem in the tuning of the radio wave frequency is an indirect evidence for the enhancement in the electrical conductivity of the activated carbon samples. Thus, upon activation with K_2CO_3 at high temperature (800 °C) in N_2 atmosphere, the carbon materials became electrically conductive making the MAS experiments difficult. The problem can be surmounted by mixing the conductive carbon sample with an insulating media such as Kaolin. The detuning of the NMR probe caused by the improvement in the electrical conductivity of the well carbonized samples can thus be eliminated.

2.1.2. XRD Studies – Phase Structure of Carbon Material

Details of phase structure and the process of graphitization of carbon materials are obtained from XRD studies. XRD patterns of carbon materials were recorded using Shimadzu XD-D1 X-ray diffractometer operated at a scan range of 0.05° with $CuK\alpha$ radiation ($\lambda = 1.5418 \text{ \AA}$) and a Ni filter. The diffraction profiles were obtained in the scan range (2θ) of 5 – 80. The XRD pattern of the char comprises two broad diffraction peaks centered at 2θ values of 10 and 22° . The broad diffraction peak at a 2θ value of 22° is characteristic of the presence of lignin component [54, 76].

The broadness of the two diffraction peaks mentioned earlier indicate the amorphous nature of the lignin in the char. The decomposition temperature of lignin is in the range of 280 – 550°. As the char is produced at 300 °C, under the synthesis conditions not all lignin decomposes. As a result the inherent lignin structure is observed in the char

Chars from lignocellulosic materials were known to comprise of an interwoven network of carbon “ribbons” containing hexagonally arrayed carbon layers – a turbostratic graphitic structure. Precursors containing hexagonally arrayed carbon, as those found in lignin, would readily reform to stable graphitic arrays. In the case of cellulose such structural advantage is missing [77].

Above a 2θ value of 27° several sharp and intense diffraction peaks are observed in the XRD profile from the char and they are a result of silica and other typical mineral matter present in the plant tissues which remain intimately bound with carbon material in the char. Treatment of the char with NaOH (10 wt.% solution) followed by HCl treatment (conc.) removed significant amount of mineral matter. NaOH treatment is effective in removing silica whereas HCl treatment is effective in the removal of alkali (Na, K), alkaline (Ca, Mg) and transition (Fe) metals which are inevitable in the chars from lignocellulosic materials [41]. The sharp diffraction peaks characteristic of such mineral matter were completely absent in the char sample produced after NaOH and HCl treatment. The effectiveness of NaOH and HCl treatment in the removal of mineral matter is also confirmed from the analysis of ash content of the original char, char treated with NaOH followed by HCl and activated carbon material obtained from K_2CO_3 activation (char: K_2CO_3 = 1:3 (wt./wt.%)). The ash content was determined by adopting ASTM standard procedure bearing the designation D2866-94. The ash content decreased from 12.7 to 4 wt.% upon treatment with base and acid in succession. Activation with K_2CO_3 followed by additional acid washing has further reduced the ash content from 4 to 1.8 wt %.

Significant changes in the XRD profiles were observed upon activation of the char with K_2CO_3 . Upon activation, in addition to the retention of the inherent lignin structure, as evident from the retention of two broad peaks centered around 2θ values of 12° and 22° , a new diffraction peak originated at a 2θ value of 43.5° which is attributable to (10) diffraction of turbostratic carbon containing small hexagonal layer units of carbon. Similar observations are known in literature [78, 79].

Beyond a char to K_2CO_3 ratio of 1:3, the intensity of the afore mentioned peak centered at 2θ value of 43.5° decreased steadily indicating the partial collapse of the

turbostratic graphitic structure leading to disordered carbon structure with hexagonal carbon layers misoriented to one another.

2.1.3. BET Sorptometry – Textural Properties of Carbon Materials

N₂ sorption studies provide information on the textural properties (specific surface area, pore volume, and the distribution of pores depending on the size) of carbon materials produced. The sorptometric analysis on the char (as synthesised material from *Calotropis Gigantea*) as well as the activated carbon materials were carried out on Sorptometric 1990 Carbo Erba sorptometer using N₂ as adsorbent at 77 K (-196 °C). Prior to the analysis, the carbon samples were out gassed at 250 °C for 12 h. The specific surface area values are derived from the isotherm using BET (Brunauer-Emmet-Teller) method. Details of texture properties of the carbon materials produced are given in Table 6. The amount (volume) of N₂ adsorbed is the highest for the carbon material obtained when the K₂CO₃ to char ratio (wt./wt.%) ratio of 3 implying the highest specific surface area value (1296 m²/g) (Table 6) for this material. Thus the optimum ratio of activating agent:char is 3 (wt./wt.%). Beyond the afore mentioned amount, the SSA as well as the pore volume only decreased.

Table 6. Effect of amount of activating agent (K₂CO₃) on the specific surface area and pore volume values of carbon materials produced from *Calotropis Gigantea*

S. No.	Sample	K ₂ CO ₃ : C (wt./wt.%)	Specific Surface Area (m ² /g)	Specific Pore Volume (cm ³ /g)
1	Char (as synthesised)	0	97	0.08
2	Activated Carbon1	1	892	0.50
3	Activated Carbon2	2	1083	0.59
4	Activated Carbon3	3	1296	0.73
5	Activated Carbon4	4	765	0.45
6	Activated Carbon5	5	922	0.53

Irrespective of the amount of the activating agent, all the activated carbon materials exhibited type I isotherms, according to Brunauer, Deming, Deming and Teller (BDDT) classification [80, 81].

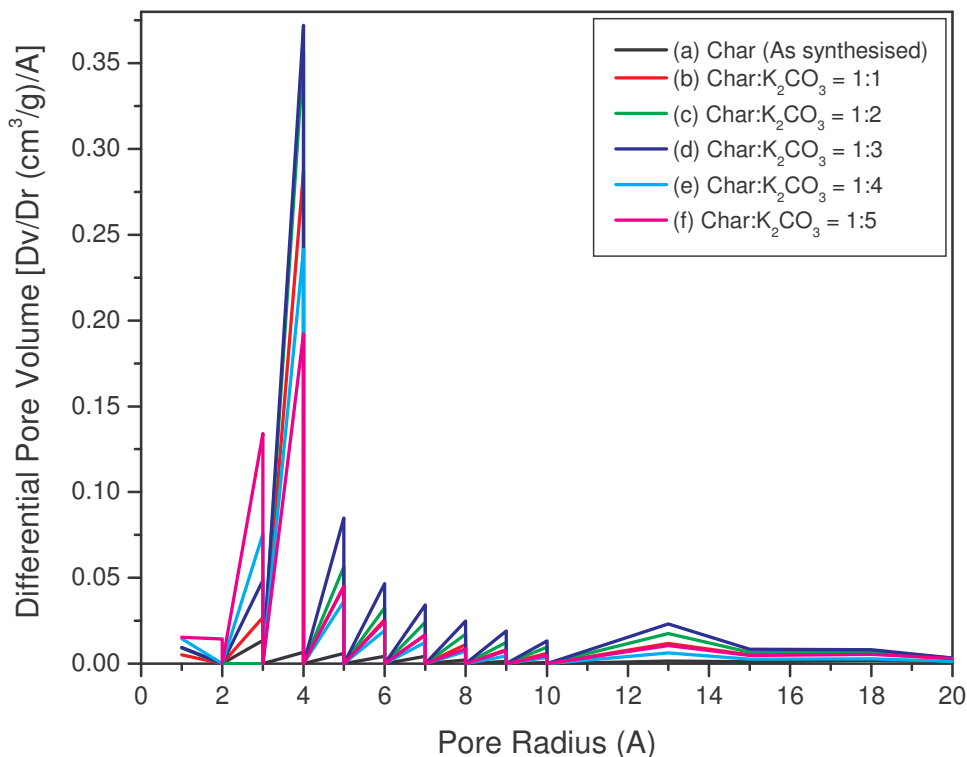


Fig. 16. Pore size distribution curves, based on Horvath-Kawazoe method, of carbon materials prepared from *Calotropis Gigantea*, (a) as synthesized (char), activated carbon with a Char to K_2CO_3 ratio (wt./wt.%) of (b) 1:1, (c) 1:2, (d) 1:3, (e) 1:4 and (f) 1:5 (reproduced from ref. 43)

Evaluation of the pore size distribution (PSD) is of importance in the characterization of microporous materials. The PSD of the char as well as the activated carbon materials produced from different K_2CO_3 to char ratios using Horvath-Kawazoe method are shown in Fig. 16. Owing to the computational simplicity, Horvath-Kawazoe (HK) method is preferred compared to the density functional theory. The impregnation ratio is found to have a profound effect on the PSD of the activated carbon materials. With an increase in the ratio up to a K_2CO_3 to char ratio of 3, the micro pore structure (pore radius between 2

to 4 Å) as well as the mesopore volume (pore radius between 10 to 15 Å), formed by the widening of the micropores, increased resulting in an increase in the total pore volume. Beyond a K₂CO₃ to char ratio of 3, the intensity of micropore volume as well as the mesopore volume decreased due to blocking of the pores. Such pore blockage by both partial collapse of the pore wall as well as by the decomposed products of the activating agent is more pronounced in the case of activated carbon produced with a K₂CO₃ : char (wt./wt.%) ratio of 4 (Fig. 16. (e)).

Up to a K₂CO₃ to char (wt./wt.%) ratio of 3, there is a tremendous increment in the amount of N₂ adsorbed indicating an increase in pore volume and specific surface area of the carbon material as a result of evolution of pores as well as widening of the existing pores. A peculiar behaviour is observed in the textural properties of the carbon material obtained at a char to K₂CO₃ ratio of 1:4 indicating a sort of transition being taking place at this stage.

Even though, all the carbon materials produced from activation with different amounts of K₂CO₃ exhibited type I isotherms indicating that all the carbon materials are microporous in nature there are significant differences in the shapes of isotherms offering valuable information. Firstly, the isotherm curves is exactly lying parallel or horizontal to the relative pressure (p/p₀) axis (X-axis) implying that the activating carbon material obtained from a char to K₂CO₃ (wt./wt.%) ratio is exclusively microporous. Major uptake occurred at a low relatively pressure (less than 0.1). This is an indication of the formation of highly microporous material with a narrow pore size distribution. Gregg and Sing [82] have attributed such complete filling of pores at very low relative pressure in the case of microporous materials to the strong interaction potential between the adsorbent and adsorbate. Also the initial steep region was abruptly followed by a plateau. This indicates that the adsorption is stopped owing to the close proximity of the pore wall preventing the formation of multilayers . Thus mesopores and macropores are absent in the case of activated carbon produced with a K₂CO₃:char ratio of 4.

The exclusive microporous nature and also the decrease in the micro and mesopore volumes in the afore mentioned case were observed in the pore size distribution (PSD) curve shown in Fig. 20. (e). In addition there is a pronounced decrease in the specific surface area value of the carbon material activated upon increasing the char to K₂CO₃

ratio from 1:3 to 1:4 (SSA decreased from 1296 to 765 m²/g) indicating blockage of micropores as well as the mesopores. Unlike the case of activation with a char to K₂CO₃ activation of 1:4, Fig. 20. (e), other isotherm curves (Fig. 19. (b), (c), (d) and (f)) exhibited appreciable slope in the isotherm in the high pressure region. Such a marginal increase in adsorbed volume in the relative pressure range of 0.35 – 0.95 with an increase in the char to K₂CO₃ ratio (wt./wt.%) from 1:1 to 1:3 can be attributed to the formation of mesopores as a result of the pore widening. Formation of such mesopores (an increase in pore volume in the range of 20 – 30 Å (pore diameter)) is observed in the PSD curves Figs. 20. (b), (c), (d) and (f).

2.1.4. Elemental Analysis – Chemical Constitution of Carbon Materials

The elemental analysis of the char, char treated with NaOH followed by HCl as well as char activated with K₂CO₃ (char:K₂CO₃ (wt./wt.%) = 1:3) was carried out on CHNS/O analyzer (Perkin Elmer Instrument, Series II) and the result is summarized in Table 7. Acetanilide was used as reference for calibrating the elemental analyzer.

Table 7. Chemical composition of carbon materials from Calotropis Gigantea

Element (wt. %)	Carbon Materials from Calotropis Gigantea		
	Char (As synthesized)	Base and Acid treated (NaOH and HCl) treated	Activated with K ₂ CO ₃ (Char:K ₂ CO ₃ = 1:3)
Carbon	73.13	77.62	80.04
Hydrogen	2.61	2.63	3.50
Nitrogen	0.81	0.82	0.67
Sulphur	0.36	0.33	0.36
Total	76.91	81.40	84.57
Ash content	12.7	4.0	1.8
Oxygen*	10.39	14.6	13.63

* By difference from the total amount of other constituents

Simple treatment of the char with NaOH (10 wt.% solution) and HCl in succession has improved the carbon content (wt.%) from 73.13 to 77.62 which is attributed to the elimination of mineral matter. Activation with K₂CO₃ has further increased the carbon content from 77.62 to 80.04 % and also the oxygen content decreased from 14.6 to 13.6

% as expected. It is interesting to note an increase in the hydrogen content from 2.63 to 3.5 wt.% upon activation which is not expected. Upon activation oxygen and hydrogen are striped off from char structure. The increase in hydrogen upon activation is not because of activation step (reaction) but because of the subsequent treatment of the activatead carbon composite (carbon material with the decomposed products of activated carbon, mainly K) with HCl and further washing with water. In fact, during the K_2CO_3 activation process surface species such as C-O-K are formed which upon treatment with HCl and subsequent washing with water gets transformed to C-O-H groups which contribute to an increase in the hydrogen content in the case of activated carbon sample relative either the original char or the base and acid treated char.

2.1.5. Effect of K_2CO_3 activation on the chemical environment and the concentration of unpaired electrons (spin density of electron) in carbon materials from Calotropis Gigantea

Electron paramagnetic (spin) resonance (EPR or ESR) spectroscopy is a technique to examine and investigate the electronic structure of carbon materials. EPR studies on carbon materials provide information on the chemical environment of the unpaired electron present in the carbon matrix [83, 84].

Table 8. g-factor, peak-to-peak separation (ΔH in Gauss) and concentration of unpaired electrons in the carbon materials produced from Calotropis Gigantea

S. No.	Carbon Material	g-factor value	ΔH (in Gauss) Peak to peak separation	Spin Concentration per gram of carbon material
1	Char (as synthesized)	2.00092	11.0	0.73×10^{19}
2	Char (base and acid treated)	1.99980	6.0	0.33×10^{19}
3	Char activated with K_2CO_3 (char: K_2CO_3 = 1:3, wt./wt.%)	2.00058	9.5	0.15×10^{16}

The EPR spectra of the char, char treated with base (NaOH) and acid (HCl) and the char activated with K_2CO_3 (char: K_2CO_3 = 1:3 (wt./wt.%)), shown in Fig. 17., were recorded on a Varian E-112, X band spectrometer at room temperature using the free radical, DPPH (diphenyl picryl hydrazyl radical) as external reference to evaluate the g factor

value as well as the concentration of the unpaired electrons in each of the carbon samples. The g factor is a dimensionless constant and is equal to 2.002319 for unbound electron (free electron). From the EPR spectra shown in Fig. 17. The g-factor values, peak to peak separation, ΔH in Gauss, and the spin concentration values were evaluated and are summarized in Table 8. The spin concentration values were determined by following the procedure described in reference [85].

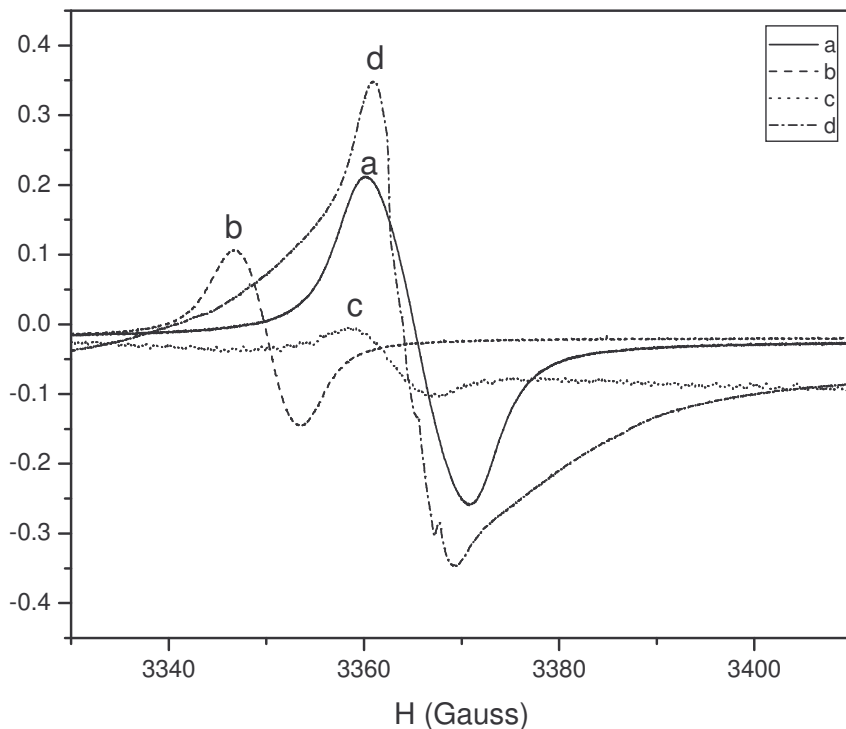


Fig. 17. EPR spectra of (a) char from *Calotropis Gigantea*, (b) char treated with NaOH followed by HCl, (c) char activated with K_2CO_3 (char: K_2CO_3 (wt./wt.%) =1:3) and (d) DPPH (diphenyl picryl hydrazyl radical)

Important details from the data derived from the EPR spectra shown in Fig.17. and summarized in Table 8 are:

(i) the g factor values of the original char, char treated with base and acid as well as the char activated with K_2CO_3 are close to the g value of the free electron (2.002312) with in the error of our experiments (± 0.002). Manivannan et al., [26], Vilas Ganpat Pol et al.,

[58], Singer and Wagoner [86], Chauvert et al., [87], Zhuo et al., [88] have made similar observations in the case of carbon materials produced from a variety of precursors.

(ii) the peak to peak separation was found to be higher in the case of original char ($\Delta H = 11.0$ Gauss) compared to either the char treated with base and acid or the char activated with K_2CO_3 . Such a broadness in the EPR signal is attributed to the presence of SiO_2 in the original char as previous revealed from XRD analysis. The decrease in ΔH value upon treatment with base and acid is an indication of the removal of silica from the char highlighting the effectiveness of the process in getting rid of silica which is usually and inherently bound intimately in the carbon matrix. As early as 1968, Singer and Wagoner [86] have made similar observation of broadening of the EPR signal resulting from graphite because of the presence of impurities like silica. Mrozowski has attributed the peak broadening to some changes in the structure of carbon material [84].

Also from the data in Table 8. it is observed that upon activation with K_2CO_3 the ΔH value increased from 6.0 to 9.5 G indicating the presence of traces of K in the carbon material after activation leading to slight broadening in the EPR signal. Chen et al., [83] have observed ΔH values of 2.0 and 1.0 G in the case of purified and shortened single walled carbon nanotubes.

(iii) The concentration of unpaired electrons in the char produced from *Calotropis Gigantia* was found to be of the order of $0.74 \times 10^{19}/g$. The origin of such spins is attributed to the generation of dangling bonds formed as result of the extensive devolatilization from the defragmentation of the hemicellulose, cellulose and lignin structure during the preparation of the char in the muffle furnace at $300^\circ C$. Paramagnetic centers were found to be associated with the dangling bonds formed during the carbonization of carbon materials [89].

The spin concentration of the graphon black and acetylene black [25] were 1.1×10^{19} and 3.8×10^{19} spin/g respectively which are of the same order of magnitude as that of the spin concentration value observed in the case of the unactivated char shown in Table 8.

Upon treatment of the char with base and acid the spin concentration decreased from 0.74×10^{19} to 0.34×10^{19} spin/g. Nearly a three orders of magnitude reduction in spin concentration is observed upon activation of char with K_2CO_3 (0.15×10^{16} spin/g). Such

a drastic decrease in spin concentration upon activation with K_2CO_3 is because of the saturation of the dangling bonds with K metal, formed during the carbothermal reduction of K_2CO_3 , resulting in the formation of surface C-K bonds which subsequently transform to C-H bonds upon final treatment with Conc. HCl. Such a transformation is also confirmed from the increase in the hydrogen content (2.63 to 3.5 wt.%) of the carbon sample activated with K_2CO_3 and subsequently treated with conc. HCl (Table 7). Manivannan et al., [26] have found the spin concentration values of activated carbon materials, namely, GX203 (from coconut shell precursor), P1400 (from wood precursor) and Med50 (from coconut shell precursor) to be 1.8×10^{17} , 5.8×10^{17} and 1.8×10^{16} spins/g respectively.

3. Effect of the nature of cation of the alkali metal carbonate on the textural properties of Activated carbon Materials

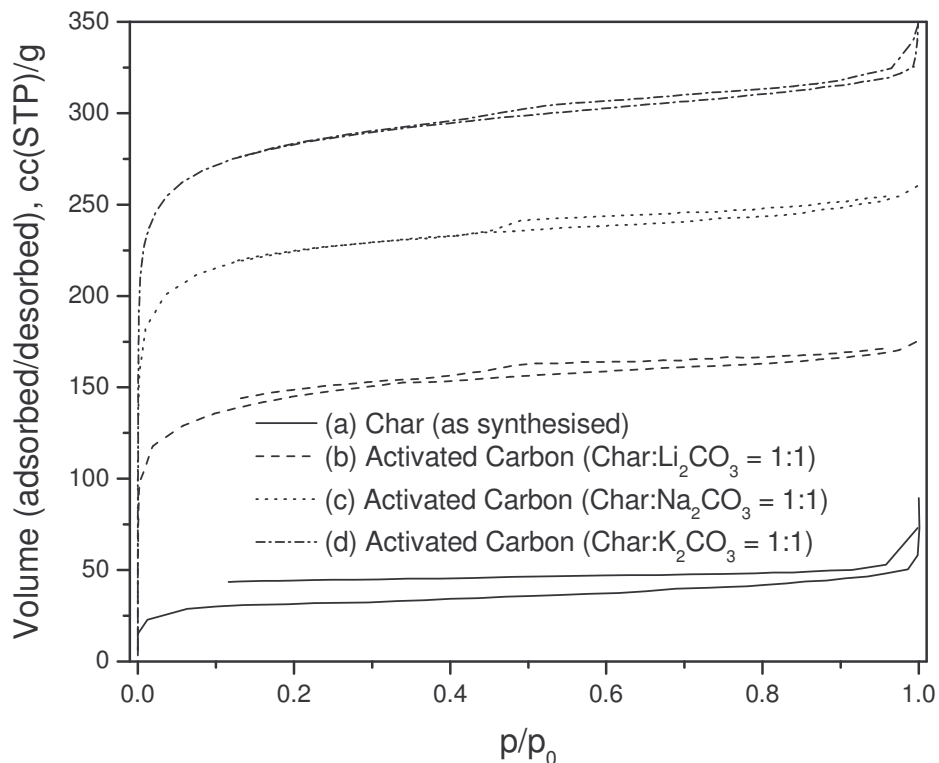


Fig. 18. N_2 adsorption-desorption isotherms of carbon materials prepared from *Calotropis Gigantea*, (a) as synthesized (char) and activated carbon with a char to activating agent ratio (wt./wt.%) of 1:1, (b) Li_2CO_3 activation (c) Na_2CO_3 activation and (d) K_2CO_3 activation (reproduced from ref. 43)

To evaluate the effect of the cation of the activating agent on the textural properties of activated carbon, the char obtained from *Calotropis gigantea* is subjected to activation with Li_2CO_3 , Na_2CO_3 and K_2CO_3 at a temperature of 800 °C for 8 h in N_2 temperature. The char:activating agent ratio was 1:1 (wt./wt.). The original char as well as the activated carbon materials were subjected to sorptometric analysis using N_2 gas as adsorbent at 77 K. The N_2 adsorption-desorption isotherms collected over the activated carbon materials obtained from activation with Li_2CO_3 , Na_2CO_3 and K_2CO_3 are depicted in Fig. 18.

Table 9. Effect of nature of cation of the activating agent on the textural properties of activated carbon

S. No.	Activating agent	Ionic radii of the cation (Å) ^a	E^0 (V) ^{b, c}	Textural properties of Carbon Materials	
				Specific Surface Area (m ² /g)	Specific Pore Volume (cc/g)
1	Li_2CO_3	0.60	-3.0	480	0.263
2	Na_2CO_3	0.96	-2.7	811	0.395
3	K_2CO_3	1.33	-2.9	892	0.497

a. & b. from ref. [75] p.197



c. The standard redox potential of activated carbon is + 0.24 V [90]

There is a steady raise in the volume of the adsorbate adsorbed on the activated carbon material as the activating agent is changed from Li_2CO_3 to K_2CO_3 through Na_2CO_3 . The specific surface area of the activated carbon produced was found to be dependent on the radii of the cation of the activating agent as shown in Table 9. It was observed that greater the cationic radii of the activating agent greater is the specific surface area of the activated carbon material.

Thus alkali metal carbonates have the potential to promote activation of carbon materials yielding high values of porosity and a corresponding high specific surface area values. Apart from transition metal salts and alkali metal carbonates the possible utility of several other chemical compounds for activating carbon materials have been investigated.

Table 10. Tuning the Textural Properties of Carbon Material – Role of Chemical Activator

S. No.	Chemical Activator	S _{BET} (m ² /g)	V _p cm ³ /g	Type of isotherm/porosity
1	Li ₂ CO ₃	478	0.26	Type I (Microporous)
2	Na ₂ CO ₃	811	0.40	Type I (Microporous)
3	K ₂ CO ₃	892	0.50	Type I (Microporous)
4	Ca(CO ₃) ₂	524	0.33	Type I (Microporous)
5	Ba(CO ₃) ₂	170	0.10	Type I (Microporous)
6	Zn(CO ₃) ₂	626	0.30	Type I (Microporous)
7	NaCl	400	0.20	Type I (Microporous)
8	NaBr	319	0.16	Type I (Microporous)
9	KBr	275	0.10	Type I (Microporous)
10	NaI	58	0.04	Type I (Microporous)
11	CaO	521	0.25	Type I (Microporous)
12	Ca(OH) ₂	189	0.11	Type I (Microporous)
13	CaCl ₂	156	0.09	Type I (Microporous)
14	Ba(OH) ₂	152	0.08	Type I (Microporous)
15	Al ₂ O ₃	174	0.17	Type IV (Mesoporous)
16	Al(NO ₃) ₃	253	0.19	Type I (Microporous)
17	Urea	439	0.21	Type I (Microporous)
18	Sodium acetate	548	0.26	Type I (Microporous)
19	Sodium oxalate	707	0.33	Type I (Microporous)
20	Sodium potassium tartarate	394	0.20	Type I (Microporous)
21	Sodium citrate	419	0.20	Type I (Microporous)
22	Sodium tartarate	394	0.20	Type I (Microporous)
23	Citric acid	127	0.07	Type I (Microporous)
24	Tartaric acid	42	0.04	Type I (Microporous)
25	Oxalic acid	317	0.14	Type I (Microporous)

The activation conditions being: Carbon precursor:Chemical activator (wt./wt. %) ratio of 1:1, Activation temperature of 800 °C, duration of activation is for 2 h. A summary of the study of potential of various chemical compounds in tuning the textural properties of carbon materials is given in Table 10. It is observed that alkali salts of carboxylic acids are as potential as alkali metal carbonates in improving the textural properties of carbon materials.

4. Catalytic Applications of Carbon Materials for the Synthesis of tert-amyl methyl ether (TAME)

4.1. Gasoline Additives for Clean Environment

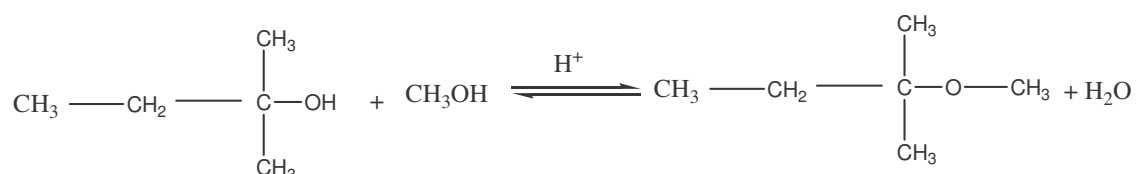
Addition of oxygenates improve the burning characteristics of fuels [91, 92]. Oxygenates (gasoline additives) are essential to increase the oxygen content of the gasoline above 2 wt.% which is required for the clean burning of fuel. Addition of oxygenates to gasoline causes reduction in CO and unburnt hydrocarbon exhaust emission. Tertiary alkyl ethers are preferred gasoline additives because of high octane numbers, low blending vapour pressure and low atmospheric reactivity. Ethers such as methyl tert – butyl ether (MTBE), ethyl tert – butyl ether (ETBE), tert – amyl methyl ether (TAME) and di isopropyl ether have attracted the attention of refiners as fuel blending components [93]. Tert – alkyl ethers play an important role in producing ecofriendly and clean fuels (blended gasoline). MTBE, widely used and cheap gasoline additive, has been found recently to be causing ground water pollution and its use is banned in many countries. As a result the focus is now switched on to alternate gasoline additives such as TAME and ETBE. The octane number of TAME (106) is close to the value of MTBE (109). The blending Reid Vapour Pressure (RVP) of TAME (1 psi) is lower than that of either MTBE (8 psi) or ETBE (4 psi) emphasizing the potential of TAME as future gasoline additive.

In general the ethers were produced from the reaction between i-amylenes or i-butylenes with alcohols (ethanol or methanol) over solid acid catalysts like Amberlyst - 15, Amberlyst – 36, ion-exchange resin beads (A 16, A 35 and XE 586) and fibrous ion exchange resin (SMOPEX – 101), 20 wt. % HPW/K-10 clay, UDCaT – 1, UDCaT – 2 [93, 94]. Even though these catalysts showed good activity, ion – exchange resins have the inherent limitation of thermal stability and loss of acid sites by leaching. Thus there

is a need for the design of catalysts for the synthesis of oxygenated fuels with performance better than the currently used ion exchange resins.

4.2.1. Design of Catalyst for the Synthesis of tert – amyl methyl ether (TAME)

In the condensation reaction of tert – amyl alcohol (TAA) and methanol water is formed as a byproduct. The catalyst need to be hydrophobic to resist leaching of the active component. Carbon materials are sufficiently hydrophobic owing to the presence of graphite like chemical properties and can form an integral component of the catalyst. Acid function is yet another component needed to drive the etherification reaction. Heteropoly acids, particularly, dodeca tungstophosphoric acid is a strong super acid with a H_0 value of – 13.4, a value lower than the H_0 value of 100 % sulphuric acid ($H_0 = -11.94$). Appropriate combination of heteropoly acid and carbon materials yields active and stable solid acid catalyst for the synthesis of TAME from TAA and MeOH.



4.2.2. Preparation of Catalyst (HPW/C) for the Synthesis of TAME

Four different carbon materials, namely, activated carbon from Calotropis Gigantea (ACCG from K_2CO_3 activation), Black Pearl, Vulcan XC 72 R and CDX 975 with varying textural properties (shown in Table 11) were employed as support material for dodeca tungstophosphoric acid (HPW) to evaluate the effect of the nature of carbon support on the activity of the supported solid acid catalyst.

Table 11. Textural Properties of Carbon Materials

S. No.	Carbon Material	Specific Surface Area (m^2/g)	Density (g/cc)	Pore Volume (cc/g)
1	CDX 975	215	0.23	0.28
2	Vulcan XC 72 R	224	0.33	0.46
3	Black Pearl 2000	1012	0.15	1.15
4	Activated Carbon from Calotropis Gigantea	1291	0.28	0.73

The HPW/C catalysts were prepared by the method of dry impregnation where in to the aqueous solutions of HPW known amount of carbon material is added and stirred at room temperature for 6 h followed by drying the catalyst at 80 C in a water bath to obtain 10 wt. % HPW/C. The catalysts prepared were designated as 10 wt.% HPW/ACCG, 10 wt. % HPW/Black Pearl 2000, 10 wt.% HPW/Vulcan XC 72 R, 10 wt.% HPW/CDX 975.

4.3. Evaluation of Catalytic Activity of HPW/C catalysts for the synthesis of TAME

The catalytic activity of carbon supported heteropoly acids was investigated using the vapour phase synthesis of TAME as a test reaction.

The reaction was carried out in a down flow fixed bed reactor at atmospheric pressure at a temperature of 373 K. The liquid feed containing tert – amyl alcohol (TAA) and methanol (in the mole ratio of 1:10) was fed onto the catalyst bed through a peristaltic pump (Miclins, SPO1) at a flow rate of 10 ml/h. N₂ is used as a carrier gas (flow rate – 30 ml/min). In a typical run 0.5 g of the catalyst was charged in the reactor. The catalyst was stacked between glass beads and ceramic wool. The reactor was maintained under isothermal conditions during all runs. The reaction products were condensed at the bottom of the reactor and analyzed for the chemical composition using gas chromatography equipped with OV 101 packed column and a FID detector.

The condensation reaction between tert - amyl alcohol and methanol over HPW/C catalysts is monitored for 3 h (Fig. 19). Reaction products were collected and analysed by GC at an interval of 30 min. The catalytic activity is evaluated by monitoring the conversion of TAA with time. In situ generation of iso amylenes (2-methyl-1- butane, 2MB1, and 2-methyl-2-butene, 2MB2) was observed during the course of reaction. The formation of iso amylenes is a result of the cracking of tert – amyl alcohol. The iso amylenes formed subsequently react with MeOH to form TAME.

Details of conversion (wt. %) of TAA and selectivity towards olefins and TAME over different HPW/C catalyst are summarized in Table 12. The values of conversion and selectivities are at the 3rd hour of the reaction. The textural properties of the carbon supports (shown in Table 12) were found to have a remarkable effect on the catalytic activity of the HPW/Carbon catalysts.

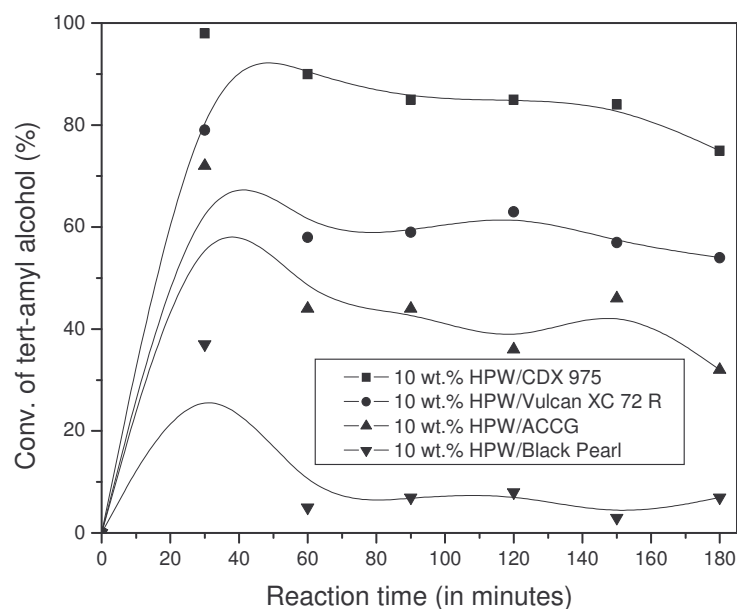


Fig. 19. Plot of Conversion of TAA (wt. %) Vs Reaction time (in minutes)

Table 12. Catalytic Activity (at 180 min of the reaction) of HPW/C catalysts for the synthesis of TAME^a

Catalyst	Conversion (wt. %) ^b	Selectivity (%)	
		Olefins	TAME
10 wt.% HPW/CDX 975	75	35	65
10 wt.% HPW/Vulcan XC 72 R	54	13	87
10 wt.% HPW/ACCG	32	37	73
10 wt.% HPW/Black Pearl 2000	7	47	53

a. Reaction Conditions:

Mole ratio of tert – amyl alcohol/methanol = 1:5

Flow rate of the feed = 10 ml/h

Flow rate of the carrier gas = 30 ml/min

Amount of catalyst = 0.5 g

b. Olefins : 2-methyl-2-butene (2MB2), 2-methyl-1-butene (2MB1)

The HPW/CDX 975 catalyst, with the lowest value of S_{BET} value of C, showed highest conversion (even after 3 h of reaction) implying that the lower S_{BET} value of the carbon support offered optimum dispersion of the active component leading to, probably, the mild acidity required for the etherification reaction unlike the HPW/Black Pearl 2000 catalyst, with high S_{BET} value of carbon support, resulting in fine dispersion of HPW crystallites and correspondingly to high acidity which is not required for the condensation reaction under the study. The catalyst prepared from the carbon material produced from the stems of Calotropis Gigantea (activated with K_2CO_3 with a char:activating agent (wt./wt.%) ratio of 1:3) showed performance similar to Vulcan XC 72 R carbon based catalyst (10 wt.% HPW/Vulcan XC 72 R). The promising catalytic activity of the of 10 wt.% HPW/ACCG is because of the exclusive microporous nature of the carbon support (from the plant source) rendering most of the smaller heteropoly acid crystallites inaccessible to the reactant molecules and there by offering only mild acidity to the reactants required for the condensation reaction. Thus the carbon material derived from plant source is a suitable substitute to either Black Pearl 2000 or Vulcan XC 72 R which are widely used commercially available carbon materials for diverse applications.

IV. CARBON MATERIALS (AS ADSORBENT) FOR ADSORPTIVE DESULPHURIZATION

1. Need for Alternate Technology for Desulphurization

Removal of organo sulphur compounds from diesel is an issue of concern from scientific, social, economic and environmental view points. Any break through achieved in desulphurization technology will have its impact on human well being. Burning of fuel (gasoline or diesel) with S contents beyond permissible limits cause ill effects on human health. Current world demands zero sulphur fuel. Production of clean fuel has always been the goal of petroleum refining industry. But refinery itself is engulfed now in the vicious circle of a host of problems that include environmental legislation, crude oil variation, product demand, economic imbalances, energy uptake, safety and process efficiency. It should not be mistaken that conventional HDS can be a panacea to the recurring problem of S specification in the transportation fuels. Newer technologies, if found promising, should be given place and adopted.

2. Conventional Hydrodesulphurization Process - Draw backs

Hydroprocessing is one of the most important steps in the petroleum refining industry. Hydroprocessing refers to a variety of catalytic processes aimed at the removal of S, N, O and aromatic compounds present in the gasoline and diesel feed stocks. $\gamma - \text{Al}_2\text{O}_3$ supported sulfided NiMo oxide is the best known commercial catalyst for hydrodenitrogenation (HDN) whereas the sulfided CoMo oxide supported on $\gamma - \text{Al}_2\text{O}_3$ is the industrial catalyst for hydrodesulphurization. The catalyst should possess strong hydrogenation function since hydrogenation is the prime reaction in both HDN and HDS processes.

Sulphur in the oil streams is removed as H_2S from the petroleum streams in the process of hydrodesulphurization (HDS) under severe conditions of reaction temperature and hydrogen pressure [95]. Even though the oxides of sulfided CoMo and NiMo supported on $\gamma - \text{Al}_2\text{O}_3$ showed excellent performance for HDS and HDN reactions respectively, the catalysts need to be sulfided a priori to achieve the active site formation. The sulphidation process is usually carried out by exposing the catalyst to the sulphur containing feed itself. There are several ways in which the sulfided CoMo and NiMo based catalysts lose the activity. Factors that cause the loss of activity are: sintering of the active phases, decomposition of the active phases, covering of the active sites by reactants or products, coking, formation of deposits of metal sulfides. Owing to the aforementioned problems, in addition to the necessity of H_2 as well as the severity of the operating conditions, there is an urgent need for the development of alternate methods of desulphurization with efficiency towards the removal of refractory compounds.

3. Refractory S Compounds in the Petroleum Feed

Typical S containing compounds present in petroleum fractions are shown in Table 13 [96]. 4, 6 dimethyl dibenzothiophene (4, 6 DMDBT) with alkyl groups close to 'S' atom is highly refractory compound to be desulphurized. 'S' species in such 'sterically' inaccessible environment are too difficult to be removed. Two parallel reaction pathways, namely, the direct desulphurization as well as the another path involving the hydrogenation step followed by desulphurization, are possible for the desulphurization of 4, 6 DMDBT on commercial oxide catalyst (either NiMoS/Al or CoMoS/Al) as depicted in Fig. 20.

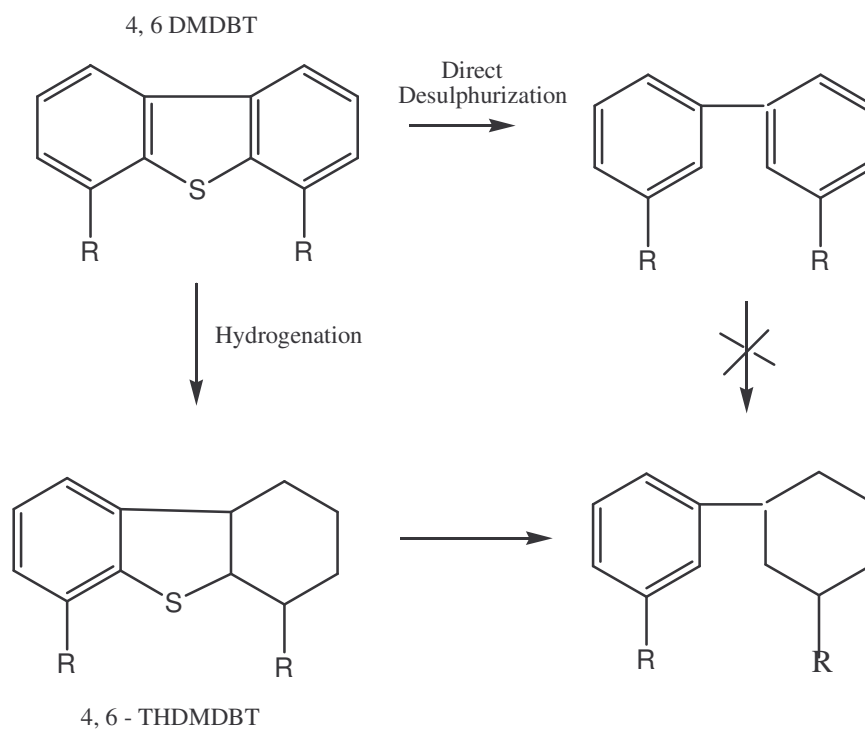
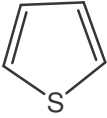
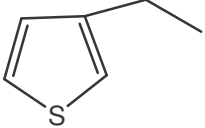
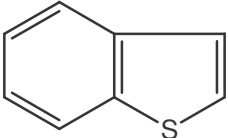
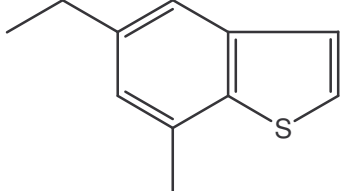
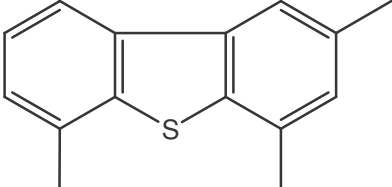


Fig. 20. Hydrodesulphurization of 4, 6 – DMDBT (R – CH₃) involving direct route and hydrogenation route (reproduced from ref. 97)

Table 13. Typical S containing compounds present in petroleum fractions

S. No.	S Compound	
	Name	Structure
1	Thiol, Mercaptan	R-SH
2	Sulfide	R-S-R'
3	Disulfide	R-S-S-R'
4	Thiophene	
5	Substituted Thiophene	
6	Benzothiophene	

7	Substituted Benzothiophene	
8	Substituted dibenzothiophene	

Direct desulphurization of 4, 6 DMDBT yields dimethyl phenyl where as the hydrogenation route initially yields dihydrobenzothiophene which is subsequently desulphurized to form methyl cyclohexyl toluene (MCHT). It was found that around 80 % of the HDS of 4, 6 – DMDBT proceeds via the hydrogenation route where in the adsorbed 4, 6 – DMDBT is first hydrogenated and then the hydrogenated compound is desulphurized [97].

The origin of refractory behaviour in compounds such as highly substituted dibenzothiophenes, 4, 6 DMDBT in particular, is related to the steric hindrance encountered for the breaking of the C-S bond. The desulphurization of 2, 6 DMDBT proceeds via two routes as shown in Fig. 21. As depicted in Fig. 21. the partial hydrogenation reaction of 4, 6 DMDBT is a common as well as primary reaction for either hydrogenation (HYD) route or direct desulphurization (DDS) route. After the formation of partially hydrogenated products, the C-S bond is cleaved in the DDS route with out any further hydrogenation. Unlike the direct desulphurization (DDS) route, in the path through hydrogenation (HYD route), complete hydrogenation of atleast one of the aromatic rings is inevitable for the C-S bond to cleave.

The presence of substituents at 4 and 6 positions of DBT hinder the β – elimination step which is necessary for the desulphurization to take place. To over come the problem of desulphurization of refractory compounds various strategies of desulphurization are being developed [98-107].

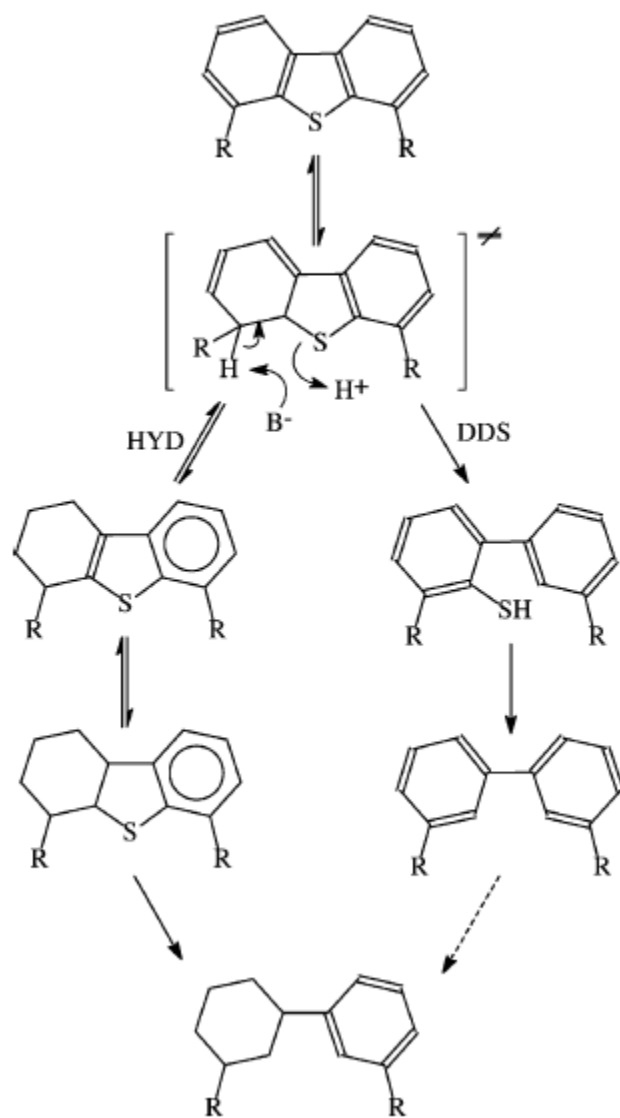


Fig. 21. Mechanism of desulphurization of substituted dibenzo thiophene

4. Recent Developments in the Process of Desulphurization

Stringent regulations are being imposed on the permissible limits of S in transportation fuel. In India the sulphur speciation is made stringent. Bharat IV norm, implying the regulation of 50 ppm sulfur by 2010, is being imposed in the selected metropolitan cities of India. Bharat III norm indicating the specification of 350 ppm of S in the diesel fuel will be implemented in places other than metropolitan cities in India. From 2000 onwards, the HDS units in many refineries are being revamped to meet the new norms.

In US from 2006 onwards, the maximum permissible limit of S in the diesel fuel is reduced to 15 ppmw. Presence of refractory sulphur compounds like, 4, 6 dimethyl dibenzothiophene, necessitate the severe operation conditions. In most of the diesel fuels, 4, 6 DMDBT, the most difficult S containing compound to be desulphurized, is present in > 100 ppm. In view of the increasing process severity of diesel HDS units to meet the upcoming stringent specifications of permissible S content, alternate methods of desulphurization are being explored. The process of oxidative desulphurization is selective in converting refractory sulphur compounds to sulfones. But the major disadvantages with the process of oxidative desulphurization are: (i) the oxidant used for the oxidative desulphurization is expensive and (ii) the separation of sulfones is an energy intensive process. Adsorptive desulphurization [102, 108-113] is an energy efficient process yielding clean fuel free from S under modest process conditions. Zeolite based adsorbents are not a viable option as such process necessitates the requirement of hydrogen for producing fuels meeting the EuroIII/IV norms. Carbon materials being multifunctional in terms of structural, textural and surface properties, they can be tuned to match the requirement for the adsorption of S containing compounds including refractory compounds.

4.1. Adsorptive Desulphurization

Viswanathan et al., [114] have developed the process for the desulphurization of SR diesel, with an initial S content of 737 ppm, from Cauvery Basin Refinery (CBR) Distillation Unit based on Adsorption. Removal of S compounds, refractory compounds in particular, is achieved under modest conditions of temperature (room temperature) and pressure (atmospheric pressure) in sharp contrast to the conventional hydrodesulphurization process where in the operating conditions are severe. The process is based on selective adsorption of organo sulphur compounds onto the tailored carbon surfaces which are employed as adsorbents. In addition to the removal of appreciable amounts of S from the SR diesel feed (430 – 450 ppm S removed from ml-diesel/g adsorbent), a simple process for the regeneration of the adsorbent bed is developed. Solvent based regeneration was found to be one of the methods yielding fresh carbon surface for further adsorption of S compounds. The regenerated bed was found to be as efficient as the fresh carbon sorbent bed. Among the cluster of activated carbon materials

tested, tailored carbon materials generated from the Adsorbent carbon (Adsorbent Carbons Pvt. Ltd., Tuticorn, India), Calgon Carbon (Tianjin Co., Ltd.) and Nuchar Carbon (MeadWestvaco, Covington, VA) were found to yield promising results for the removal of S compounds from SR diesel.

The physicochemical properties of SR diesel from Cauvery Basin Refinery are summarized in Table 14. Several commercially available activated carbon materials of varying physical and chemical properties were tested as adsorbents for the removal of organo sulphur compounds from SR diesel from Cauvery Basin Refinery Distillation unit. Among them, adsorbent carbon (A) was purchased from Adsorbent Carbons Pvt. Ltd., Tuticorn. Calgon carbon (B) was purchased from Calgon Carbon (Tianjin) Co. Ltd., Activated carbons, IG 18 x 40, IG 12 x 40 and IG 8 x 30 were purchased from Indo German Carbon Ltd., Kerala. Activated carbons, AC 4 x 8, AC 6 x 12, AC 12 x 30 were purchased from Active Carbon Pvt. Ltd., Hyderabad.

Table 14. Physicochemical Characteristics of SR diesel from CBR distillation unit

S. No.	Property	Value
1	Total Sulphur content (in ppm)	737
2	Flash Point (°C)	93
3	Aniline Point (°C)	81
4	Viscosity (at 40 °C in cSt)	4.04
5	Pour Point (°C)	+6
6	Density (g/cc)	0.8553
7	Diesel Index	60
8	Cetane Index	53

4.2. Experimental Set up for Sulphur Adsorption

A simple, inexpensive and efficient process for desulphurisation is designed. The potential of the afore mentioned carbon materials was tested. In a typical experiment the glass column of length 50 cm and internal diameter 1.5 cm is packed with 5.0 g of sorbent carbon column with glass beads on either sides. Deisel is fed on to the sorbent bed in the column through a burette at the slowest flow rate possible. The first 20 ml

product collected at the bottom of the column (out let) was analyzed for S. From the S content remaining in the product and subtracting the same from the S content in the feed diesel (737 ppm), the S content adsorbed (removed) by the carbon sorbent is obtained. Lower the S content in the product obtained through the sorbent column, higher is the sorption capacity of the activated carbon under test. The carbon materials are thus screened. Adsorbent carbon and Calgon carbon showed good performance for the adsorption of S compounds in the SR diesel (Table 15).

Different commercially available activated carbons, namely, IG 18 x 40, IG 12 x 10, IG 8 x 30, AC 4 x 8, AC 6 x 12, Ac 12 x 30, calgon carbon as received and adsorbent carbon as received were used as adsorbents for S containing compounds present in SR diesel. The results obtained on the studies with the afore mentioned adsorbents are given in Table 15. The amount of S removed (in ppm) from 20 ml deisel by 5.0 g of sorbent is shown in extreme right column of Table 2. Among the eight carbons studied Adsorbent carbon as received and Calgon carbon as received showed outstanding performance by adsorbing 229 and 181 ppm of S. So Adsorbent carbon (A) and Calgon carbon (B) were selected and further studies of adsorptive desulphurisation were carried out on these adsorbents.

Table 15. S sorbing ability of different commercial activated carbon materials

S. No.	Activated Carbon as Sorbent	*ml-diesel treated/g of adsorbent	S removed (ppm)
1	IG 18 x 40	4	134
2	IG 12 x 10	4	81
3	IG 8 x30	4	76
4	AC 4 x 8	4	12
5	AC 6 x 12	4	73
6	AC 12 x 30	4	92
7	Calgon carbon as received	4	181
8	Adsorbent carbon	4	229

* 20 ml initial product collected from the column packed with 5.0 g activated carbon and analyzed for S analysis

4.3. Activation of Adsorbent carbon (A) and Calgon carbon (B):

4.3.1. Activation with Conc. HNO₃

HNO₃ treatment changes the surface chemistry of carbon materials. Such oxidative treatment results in the formation of oxygen containing surface functional groups (carbonyl and carboxyl). The presence of such surface functional groups, in most cases, enhances the adsorption capacity of carbon materials [115, 116].

Two commercial activated carbon materials, namely, the adsorbent carbon (A) and the calgon carbon (B) were treated with conc. HNO₃. The wt./wt.% ratio of carbon to conc. HNO₃ was 1:5. The oxidative treatment of carbon with conc. HNO₃ was carried out at 60 °C for 2 hs under refluxing conditions in a 2 litre RB flask. The contents are then cooled to room temperature, washed with water and dried at 110 °C for 2 h.

4.3.2. Activation under Ar atmosphere

Ar activation involves the thermal activation of nitric acid treated carbon materials A and B at a temperature of 800 C under Ar atmosphere for 2 h in a cylindrical quartz tube.

The carbon samples after activation were termed as nitric acid treated Ar activated carbon materials.

4.4. Selected Sorbents for Adsorptive Desulphurization

Desulphurisation studies carried out with 5.0 g batch using adsorbent carbon, nitric acid treated adsorbent carbon and nitric acid treated Ar activated adsorbent carbon, calgon carbon, nitric acid treated calgon carbon and nitric acid treated Ar activated adsorbent carbon have been extended to 10.0 and 15.0 g batches. The process of adsorptive desulphurization has also been scaled upto 100 g batch using the same experimental set of glass column packed. In a typical process, diesel is continuously fed from a burette in to the column packed with the adsorbent. The product diesel is collected in aliquots of 20 ml at the bottom of the column. The S content in the product is analyzed by using *Oxford XRF analyzer*. The feed and the product diesel were also characterized for the detailed sulphur component analysis using *GC-PFPD (Gas Chromatography – Pulsed Flame Photometric Detector)*.

4.5. Characterization of Adsorbents for Desulphurization Application

4.5.1. XRD Analysis

Details of phase structure of carbon materials are obtained from X-ray diffraction studies.

X-ray diffraction patterns of adsorbent carbon as received, adsorbent carbon treated with conc. HNO₃ and adsorbent carbon treated with HNO₃ followed by subsequent

activation in Ar atmosphere were shown in Figs. 22 (a), (b) and (c) respectively . Two broad diffraction peaks centered at 2θ values of 25.4 and 43.4 were observed in adsorbent carbon as well as modified adsorbent carbons. The two afore mentioned peaks can be indexed to (002) and (101) planes of crystalline hexagonal graphite lattice respectively [(JCPDS-41-1487), 117]

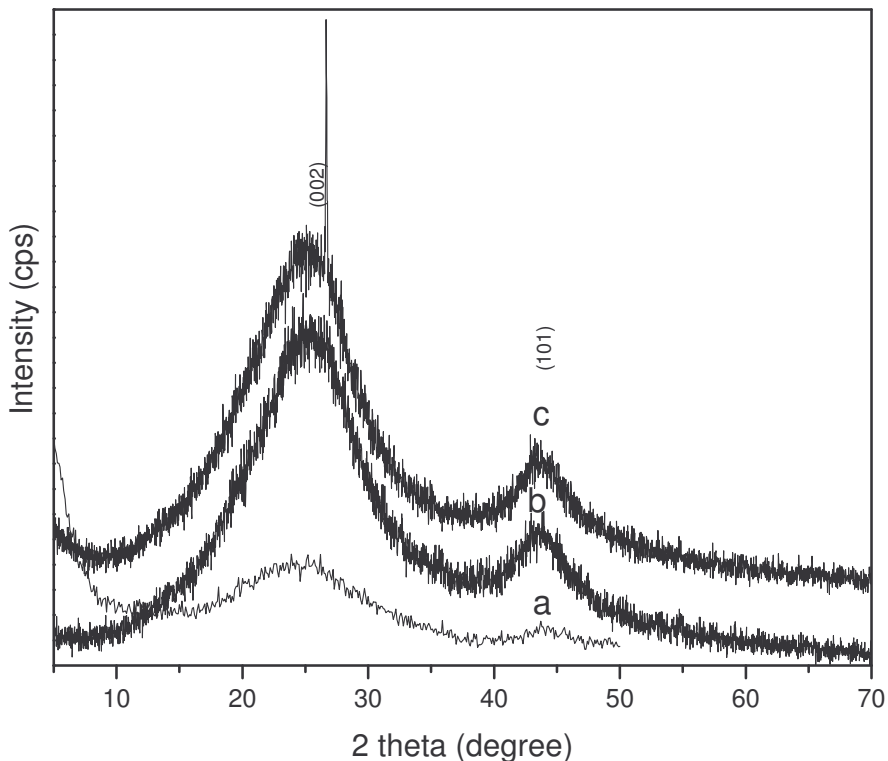


Fig. 22. XRD pattern of (a) Adsorbent carbon as received, (b) Adsorbent carbon treated with HNO_3 and (c) Adsorbent carbon treated with HNO_3 and activated with Ar

The phase structure of adsorbent carbon remained unaltered upon nitric acid treatment (Figs. 22 (a) and (b)). But in the case of adsorbent carbon treated with nitric acid followed by activation in Ar atmosphere an additional intense and narrow diffraction peak is seen at $2\theta = 26.7$ (Fig. 22 (c)). This is attributed to (002) reflection from highly crystalline graphitic carbon [118]. Nitric acid treated Ar activated adsorbent carbon (Fig. 22 (c)) is more crystalline than either adsorbent carbon as received or adsorbent carbon

treated with nitric acid alone. Thus Ar activation improved the crystallinity of nitric acid treated adsorbent carbon.

X-ray diffraction patterns of calgon carbon as received, calgon carbon treated with HNO_3 and calgon carbon treated with HNO_3 followed by Ar activation were shown in Figs. 23. (a), (b) and (c) respectively. The diffraction peaks arising from each of the afore mentioned carbon samples were indexed and are typical of graphitic carbon structure [118].

Neither HNO_3 treatment (Fig. 23 (b)) nor HNO_3 treatment with subsequent Ar activation (Fig. 23 (c)) altered the structure of original Calgon carbon sample (Fig. 23 (a)). Thus either HNO_3 treatment or Ar activation has no effect on the phase structure of calgon carbon.

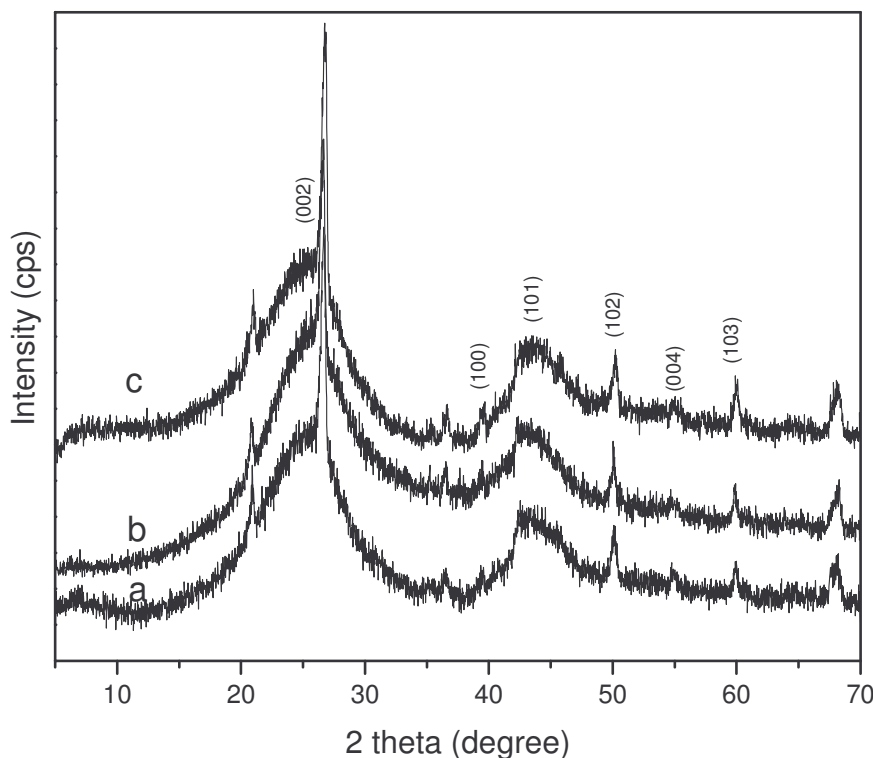


Fig. 23. XRD pattern of (a) Calgon carbon as received, (b) Calgon carbon treated with HNO_3 and (c) Calgon carbon treated with HNO_3 followed by Ar activation

There is a marked difference in the structural order between adsorbent carbon and calgon carbon (Figs. 22 and 23). No diffraction peaks resulted from adsorbent carbon or

modified adsorbent carbon beyond $2\theta = 50^\circ$ (Fig. 22) in sharp contrast to the characteristic diffraction peaks resulting from calgon and modified calgon carbon above $2\theta = 50^\circ$. Thus calgon based carbons are structurally more ordered than adsorbent based carbons.

4.5.2. BET Sorptometric Studies

Details of pore structure of carbon materials were obtained from N_2 sorption studies. N_2 adsorption-desorption isotherms of adsorbent carbon, modified adsorbent carbon, calgon carbon and modified calgon carbon are shown in Fig. 24.

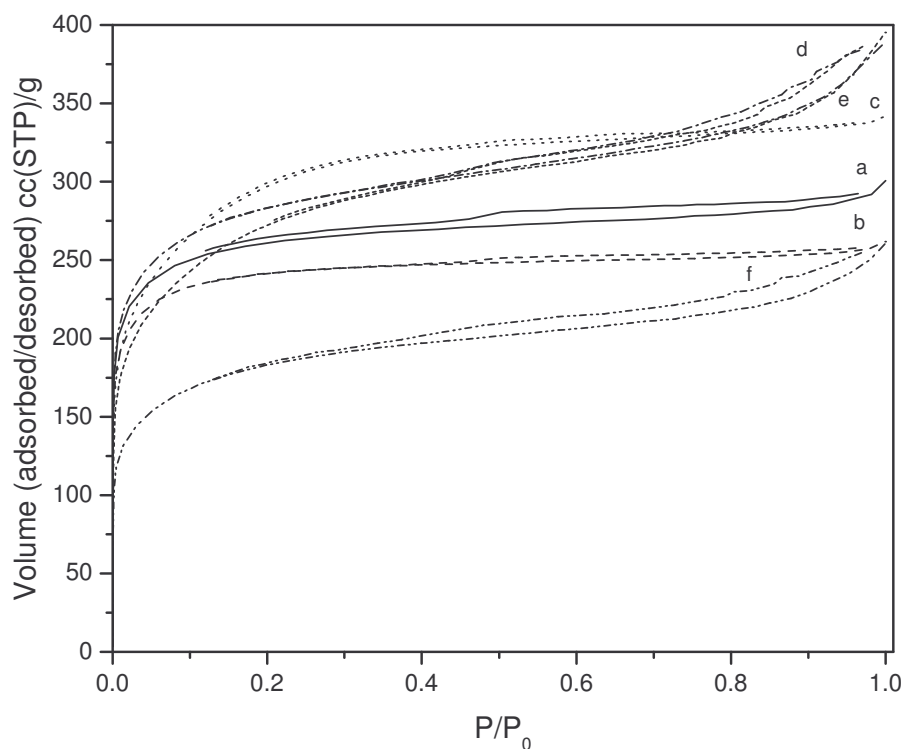


Fig. 24. Nitrogen adsorption-desorption isotherms of (a) Adsorbent carbon as received, (b) Adsorbent carbon treated with HNO_3 , (c) Adsorbent carbon treated with HNO_3 followed by Ar activation, (d) Calgon carbon as received, (e) Calgon carbon treated with HNO_3 and (f) Calgon carbon treated with HNO_3 followed by Ar activation

The N_2 adsorption-desorption isotherms arising from adsorbent carbon as received (Fig. 24 (a)), HNO_3 treated adsorbent carbon (Fig. 24 (b)) and HNO_3 treated Ar activated

adsorbent carbon (Fig. 24 (c)) are of typical type I isotherms in nature which are characteristic of microporous materials as per IUPAC classification [82].

The afore mentioned adsorption curves rose sharply at relative pressure upto 0.10. Beyond this value of p/p_0 the isotherms presented a plateau with increasing relative pressure. Also the adsorption and desorption branches were parallel over a wide range at higher relative pressure. This is an indication of the narrow pore size distribution in microporous materials with slit-like or plate-like pores [119].

The shape of isotherms presented by calgon carbon as received (Fig. 24 (d)), calgon carbon treated with HNO_3 (Fig. 24 (e)) and calgon carbon treated with HNO_3 followed by Ar activation (Fig. 24 (f)) are distinctly different from the Type I isotherms resulted from adsorbent and modified adsorbent carbons (Figs. 24 (a), (b) and (c)).

Table 16. Porosity characteristics of adsorbent, modified adsorbent, calgon and modified calgon carbon materials

Carbon Sorbent	Specific Surface Area Values (m^2/g)	Total Pore Volume (cm^3/g)
Adsorbent carbon as received	950	0.451
Adsorbent carbon treated with Conc. HNO_3	882	0.398
Adsorbent carbon treated with Conc. HNO_3 followed by Ar activation	1048	0.523
Calgon carbon as received	1014	0.587
Calgon carbon treated with Conc. HNO_3	649	0.387
Calgon carbon treated with Conc. HNO_3 followed by Ar activation	996	0.598

The isotherms resulting from calgon and modified calgon carbon samples are a combination of type I and type II isotherms. Such isotherms indicate pore structure which is a combination of micropores and mesopores. Presence of such mesopores in addition to micropores enhance the adsorption capacity for relatively large adsorbate molecules [120, 121]. The textural properties of modified carbon materials is summarized in Table 16.

4.5.3. FT – IR studies

Details of oxygen containing surface functional groups on the surface of carbon materials are obtained from FT-IR studies. The FT-IR spectra of adsorbent carbon as received, adsorbent carbon treated with HNO₃ and adsorbent carbon treated with HNO₃ followed by Ar activation are shown in Figs. 25. (a), (b) and (c) respectively.

The main distinguishing feature observed in the carbon samples after nitric acid treatment is the presence of shoulder at 1749 cm⁻¹ (Fig. 25 (b)). This is a result of stretching vibration of C=O bond in aldehydes, ketones, lactones or carboxyl groups. Thus upon nitric acid treatment C=O group is generated on the adsorbent carbon surface which is absent otherwise. Also the afore mentioned shoulder at 1749 cm⁻¹ became intense and developed in to sharp peak upon activation in Ar atmosphere (Fig. 25 (c)) [122, 123].

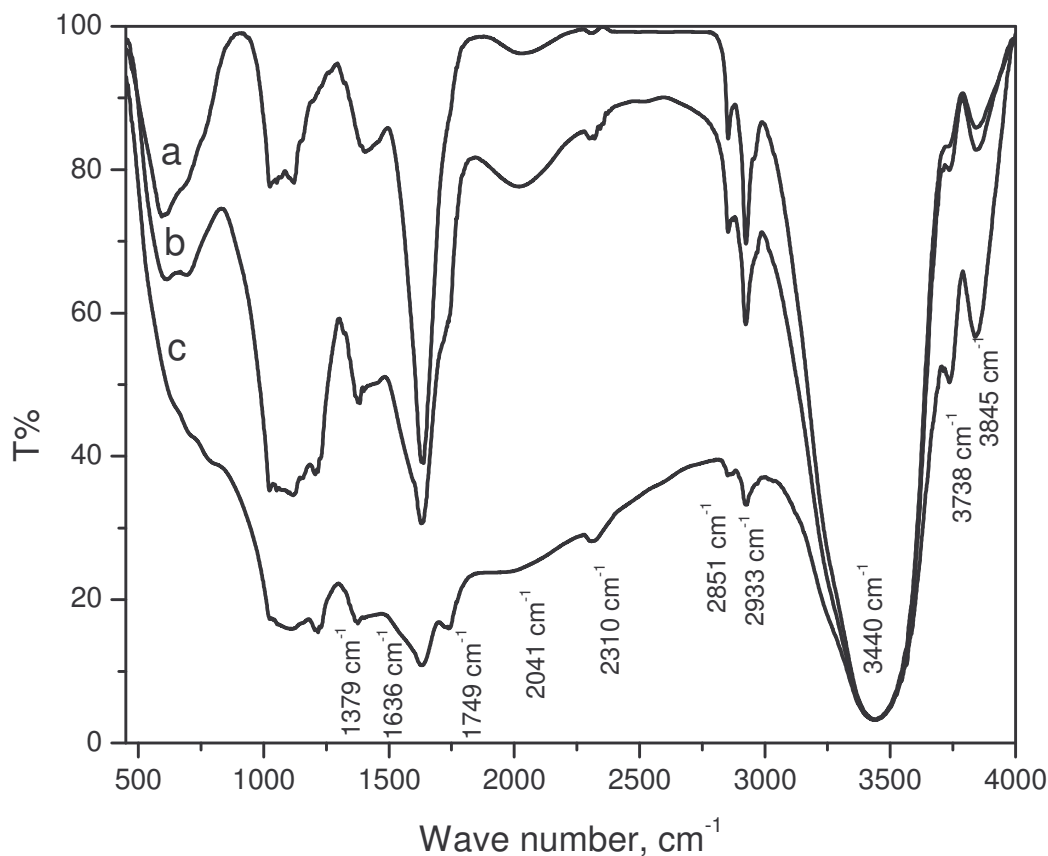


Fig. 25. FT-IR spectra of (a) Adsorbent carbon as received, (b) Adsorbent carbon treated with HNO₃ and (c) Adsorbent carbon treated with HNO₃ and activated with Ar

But for this difference all the three samples showed similar but rich surface chemistry with a variety of oxygen containing functional groups. The following functional groups are common to adsorbent carbon as well as modified adsorbent carbon (Figs. 25 (a), (b) and (c)): A sharp band at 3738 cm^{-1} is ascribed to isolated OH groups. A wide, intense band in the range of $3200\text{-}3600\text{ cm}^{-1}$ with a maximum at about 3440 cm^{-1} is assigned to the O-H stretching mode of hydroxyl groups and adsorbed water [124].

Two sharp, narrow and intense bands at 2922 and 2855 cm^{-1} are a result of asymmetric and symmetric C-H stretching vibrations of methylene group respectively [121, 125, 126]. It is to note that the peak resulting from the asymmetric C-H stretching of methylene group is more intense than that arising from the symmetric stretching of methylene group. A sharp intense peak at 1640 cm^{-1} is attributed to the carbonyl groups in quinone. Broad bands observed in the range of $1300\text{ - }1000\text{ cm}^{-1}$ are attributed to C-O stretching in acids, alcohols, phenols, ethers and esters. Broad bands in the range of $600\text{ - }800\text{ cm}^{-1}$ are a result of the out of plane deformation mode of C-H in various substituted benzene rings [121, 124].

FT-IR spectra of calgon carbon as received, calgon carbon treated with Conc. HNO_3 and calgon carbon treated with Conc. HNO_3 followed by Ar activation are shown in Figs. 26 (a), (b) and (c) respectively. There are striking differences in the surface chemistry (functionality) among the afore mentioned samples. This indicates that each of the methods of activation, whether it be HNO_3 treatment or Ar activation, has got a specific role to play and to induce surface transformation. Upon activation with Conc. HNO_3 several new bands originated at wave numbers corresponding to 3790 , 2305 and 1387 cm^{-1} which can be attributed to isolated O-H groups, ketone surface groups [127] and the in-plane bending vibration of C-H in methyl group [61] respectively (Fig. 26 (b)). In addition to the generation of -OH, C=O and $-\text{CH}_3$ groups, a broad featureless shoulder is observed in the range $2910\text{-}2990\text{ cm}^{-1}$ which is a result of aliphatic C-H stretching in methylene and methyl groups.

Ar activation of Conc. HNO_3 treated calgon carbon induced certain specific changes in to the spectral features. The first and foremost change in the appearance of a broad shoulder at 1753 cm^{-1} attributable to the origin of C=O group of carboxylic acid Fig. 26 (c). Also the broad featureless shoulder presented by HNO_3 treated calgon carbon in the

range 2910-2990 cm^{-1} developed into two clear sharp peaks centered at 2956 and 2918 cm^{-1} which are attributed to the asymmetric and symmetric stretching vibrations of C-H in methylene groups indicate the fact that Ar activation results in the generation of hydrophobic methylene C-H groups on the surface of calgon carbon which are otherwise absent. In spite of the several striking changes brought about, as discussed above, into the surface functionality of calgon carbon upon treatment with conc. HNO_3 and subsequent Ar activation, some inherent functional groups of parent calgon carbon remained unaltered even after modification. The spectral features common to all the three samples shown in Figs. 26 (a), (b) and (c) are as follows: the broad intense transmission peak centered at 3450 cm^{-1} corresponding to OH stretching mode of hydroxyl groups and adsorbed water and the broad intense peak centered at 1075 cm^{-1} which can be attributed to C-O stretching in acids, alcohols, phenols, ethers and esters [125].

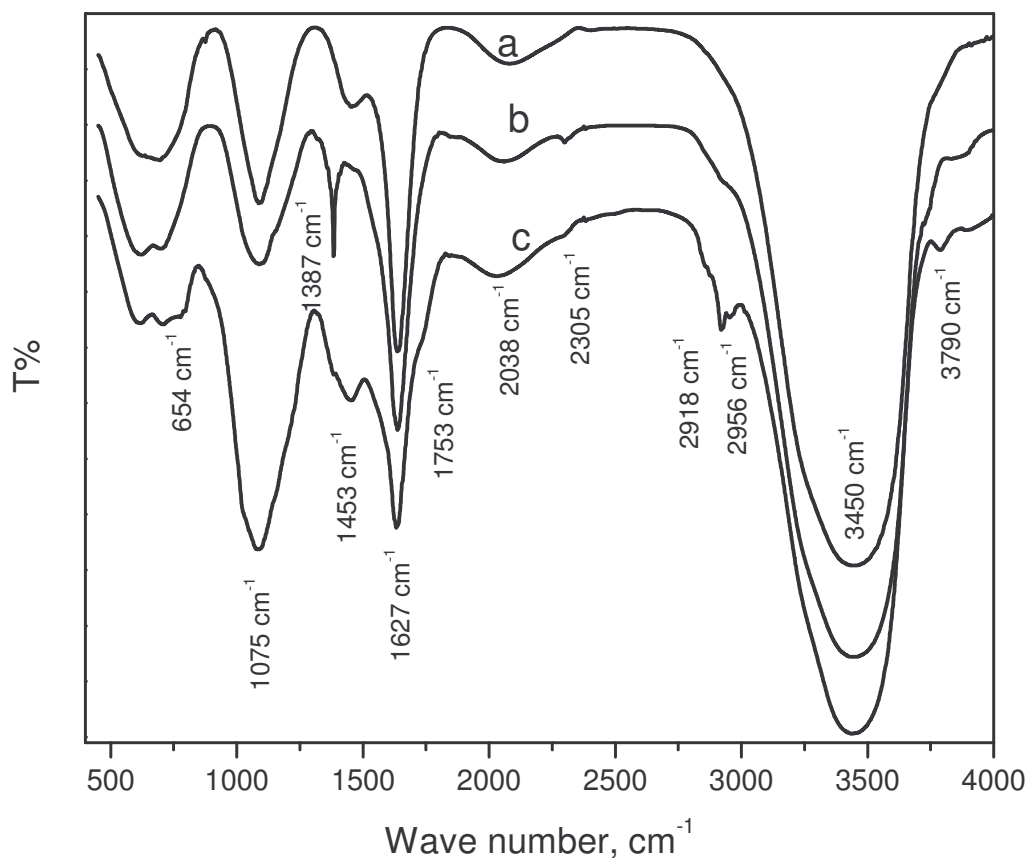


Fig. 26. FT-IR spectra of (a) Calgon carbon as received, (b) Calgon carbon treated with HNO_3 and (c) Calgon carbon treated with HNO_3 followed by Ar activation

Thus a variety of surface functional groups, namely, the hydrophilic groups such as C=O (carboxylic and ketonic), isolated -OH groups and hydrophobic C-H groups of methylene were generated on the calgon carbon surface upon treatment with conc. HNO₃ and subsequent activation in Ar atmosphere. Interestingly such a transformation in surface chemistry is achieved by keeping intact the inherent surface functionality of parent calgon carbon (Fig. 26 (a)).

4.5.4. SEM Analysis – Surface Morphology

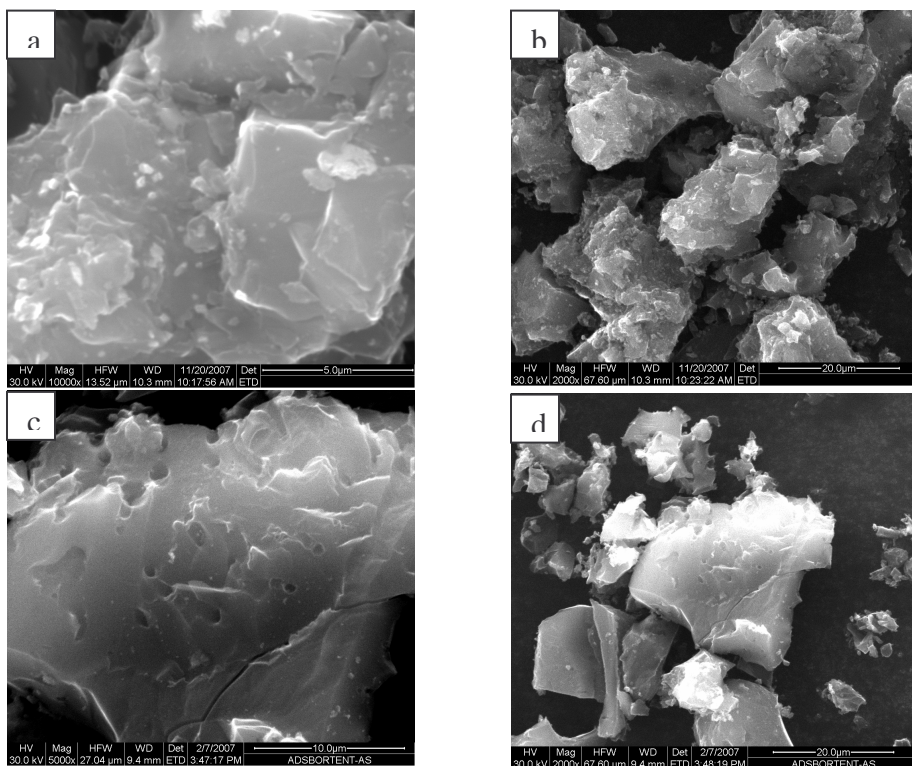


Fig. 27. SEM images (a) calgon carbon as received (magnification - 10, 000 x), (b) calgon carbon as received (magnification - 2, 000 x), (c) adsorbent carbon as received (magnification – 10, 000 x) and (d) adsorbent carbon as received (magnification - 2,000 x)

Details of surface microstructure of calgon carbon (as received) and adsorbent carbon (as received) are obtained from the scanning electronic microscopic studies. SEM images facilitate direct observation of the surface morphological features of adsorbents. SEM

images of calgon carbon as received at two different magnifications namely 10, 000 x and 2, 000 x are shown in Figs. 27 (a) and (b). The calgon carbon particles possess slate like morphology. The surface of calgon carbon is highly heterogeneous and rough with steps, kinks, edges and terraces.

SEM images of adsorbent carbon as received are recorded at two different magnifications namely 10, 000 x and 2000 x . The two afore mentioned images are depicted in Fig. 27 (c) and (d) respectively. There is close resemblance between the surface morphology of adsorbent carbon as received (Fig. 27 (c, d)) and calgon carbon as received (Fig. 6 (a, b)). Both the carbon materials possess slate like particle morphology. But the surface of adsorbent carbon (Fig. 27 (c)) is relatively smoother than that offered by calgon carbon (Fig. 27 (a)). Unlike calgon carbon surface (Fig. 27 (a)), some porous network which in its incipient stage is seen on the surface of adsorbent carbon (Fig. 27 (c)).

4.6. Evaluation of Adsorptive Desulphurization Potential of Adsorbent and Calgon based Carbon Materials

Table 17. Comparison of the S sorption capacity of Adsorbent carbon as received, Adsorbent carbon treated with HNO₃, Adsorbent carbon treated with HNO₃ followed by Ar activation, Calgon carbon as received, Calgon carbon treated with HNO₃, Calgon carbon treated with HNO₃ followed by Ar activation

Sorbent Amount	5.0 g	10.0 g	15.0 g
Sorbent Type	S removed*, (in ppm)		
Adsorbent carbon as received	229	380	410
Adsorbent carbon treated with HNO ₃	105	186	577
Adsorbent carbon treated with HNO ₃ followed by Ar activation	346	518	586
Calgon carbon as received	181	371	451
Calgon carbon treated with HNO ₃	280	378	488
Calgon carbon treated with HNO ₃ followed by Ar activation	340	399	619

* The product under consideration is the first 20 ml diesel obtained through the sorbent bed

* S content in the diesel feed – 737 ppm

Adsorbent carbon as received, adsorbent carbon treated with HNO₃, adsorbent carbon treated with HNO₃ followed by Ar activation, calgon carbon as received, calgon carbon treated with nitric acid, calgon carbon treated with nitric acid followed by Ar activation were all employed as sorbents for S removal from SR diesel.

The adsorptive desulphurization process was carried out using the afore mentioned sorbents at three different batch scales, namely, 5.0 g, 10.0 and 15.0 g. S sorption increased linearly as the amount of sorbent employed increased from 5 to 15 g irrespective of the sorbent used. Also nitric acid treatment and subsequent Ar activation greatly enhanced the S adsorption ability of both adsorbent carbon and calgon carbon. It is observed from the data presented in Table 17. that to derive the best from the oxidative treatment of carbon material, either adsorbent carbon or calgon carbon, subsequent activation in Ar atmosphere is a must.

Table 18. Type and amount of the S compounds in the feed and the product diesel (after passing through the carbon bed) as analyzed by GC – PFPD

Sulphur Species	S content (in ppm)		
	CBR diesel (Feed)	Adsorbent carbon HNO ₃ followed by Ar treatment, 15.0 g	Calgon carbon, HNO ₃ followed by Ar treatment, 15.0 g
C ₁ BT	4.6	Nil	Nil
C ₂ BT	119.6	Nil	Nil
C ₃ BT	137.5	75.2	67.2
C ₃ ⁺ BT	79.6	68.9	47.4
DBT	91.5	2.6	1.3
C ₁ DBT	157.7	Nil	Nil
C ₂ DBT	116.7	Nil	Nil
C ₃ DBT	29.5	4.3	2.1
Total S	737	151	118

*C₁, C₂, C₃, C₃⁺ BT and DBT - mono, di, tri and multi alkyl substituted benzo thiophene and di benzo thiophene

Combination of nitric acid treatment and Ar activation induces suitable surface functionality (discussed under FT-IR section), polarity (surface hydrophilic and hydrophobic functional groups), phase structure (discussed under XRD) and pore structure (discussed under BET sorptometry) into the carbon adsorbents facilitating enhanced adsorption for organo sulphur compounds present in the diesel feed stocks.

The adsorptive desulphurization process utilizing carbon materials (activated by the method which is a combination of nitric acid treatment and Ar activation) as adsorbents is efficient and potent not only in terms of eliminating significant amounts of S from the feed as shown in Table 17. but also the carbon materials are potential adsorbents for the removal of refractory S compounds (Table 18). The nature of S components present in the product diesel was analyzed using GC – PFPD and the results obtained over 15.0 g sorbent bed using modified Adsorbent carbon (A) and Calgon carbon (B) are shown in Table 18. It is observed that the the most highly refractive compounds (C₂BT and C₂DBT) present in the feed prior to desulphurization process are absent in the product diesel after the adsorption process exemplifying the utility and usefulness of the process.

4.7. Scaling up studies on s sorption - 100 g batch:

Table 19. S adsorption studies on 100 g Adsorbent carbon HNO₃ treated, Ar activated and Calgon carbon as received

S. No.	ml-diesel/g adsorbent	S content in the product (S content removed) (in ppm)	
		Adsorbent carbon activated with HNO ₃ followed by Ar activation	Calgon carbon as received
1	0.2	13 (724)	137 (600)
2	0.4	68 (669)	192 (545)
3	0.6	110 (627)	233 (504)
4	0.8	169 (568)	302 (435)
5	1.0	194 (543)	302 (435)
6	1.2	233 (504)	313 (424)
7	1.4	263 (474)	317 (420)
8	1.6	290 (447)	379 (358)
9	1.8	325 (412)	444 (293)
10	2.0	375 (362)	457 (280)
11	2.2	415 (322)	479 (258)
12	2.4	443 (294)	520 (217)
13	2.6	463 (274)	557 (180)
14	2.8	486 (251)	567 (170)
15	3.0	496 (241)	519 (218)
16	3.2	505 (232)	532 (205)
17	3.4	510 (227)	548 (189)

Apart from 5.0, 10.0, 15.0 g batches the process has been scaled up to 100 g batch too. But only two representative sorbents were tested, namely, calgon carbon as received and

adsorbent carbon treated with HNO₃ and activated in Ar atmosphere. The result obtained from desulphurization studies are shown in Table 19. Diesel with S content less than 50 ppm and 200 ppm were obtained using adsorbent carbon treated with nitric acid followed by Ar activation and Calgon carbon as received which is a remarkable break through. Even after passing 3.4 ml diesel per gram of adsorbent, nearly 200 ppm of S is being removed from diesel feed indicating the effective function of the tailored carbon based adsorbents produced.

4.8. Regeneration of Adsorbent:

Table 20. Comparison of the performance of fresh and regenerated sorbent (100 g Calgon carbon as received) for S sorption

S. No.	100 g Calgon as received ml-diesel/g adsorbent	S content in the product (S removed) in ppm	
		Fresh sorbent	Regenerated sorbent
1	0.2	137 (600)	97 (640)
2	0.4	192 (545)	110 (627)
3	0.6	233 (504)	162 (575)
4	0.8	302 (435)	256 (481)
5	1.0	302 (435)	297 (440)
6	1.2	313 (424)	370 (367)
7	1.4	317 (420)	387 (350)
8	1.6	379 (358)	443 (294)
9	1.8	444 (293)	505 (232)
10	2.0	457 (280)	512 (225)
11	2.2	479 (258)	548 (189)
12	2.4	520 (217)	549 (188)
13	2.6	557 (180)	551 (186)
14	2.8	567 (170)	554 (183)

The carbon materials (adsorbent carbon, modified adsorbent carbon materials, calgon carbon and modified calgon carbon materials) employed for adsorptive desulphurization were found to be completely regenerable. The activity of the spent sorbent is regenerated by a simple process of elution with toluene. The performance of the regenerated sorbent bed is similar to that of the fresh adsorbent bed indicating the usefulness of the developed regeneration process.

Solvent (Toluene) based regeneration method is employed. The spent sorbent used is the 100 g calgon carbon as received upon which desulphurization studies were

previously carried out (3rd column of Table 20). The toluene solvent (500 ml) used to flush the spent sorbent is collected at the out let in the batches of 100 ml and labeled as T1, T2, T3, T4 and T5. The S content in T1, T2, T3, T4 and T5 are respective 757, 275, 81, 173 and 474. Thus essentially the spent sorbent is made S free as toluene played an effective role in desorbing the adsorbed S compounds. The sorbent bed is then dried and used subsequently for next run of desulphurization.

Adsorptive desulphurization studies were then carried out on the regenerated sorbent bed. Diesel is fed through the column and the product diesel is collected from time to time in the amounts of 20 ml per batch at the outlet and analysed for S content. The process is stopped when S content of the outlet becomes equal to the S content of the feed. The S sorption results obtained on regenerated 100 g calgon carbon as received are presented in Table 20. For easy comprehension of the relative performance of fresh and regenerated sorbents the data in Table 20 is represented pictorially in Fig. 28. It is evident from the curves shown in Fig. 28. that regenerated sorbent's performance is on a par with that of the original fresh calgon carbon as received. Thus an efficient, economic and environmentally benign regeneration method is developed.

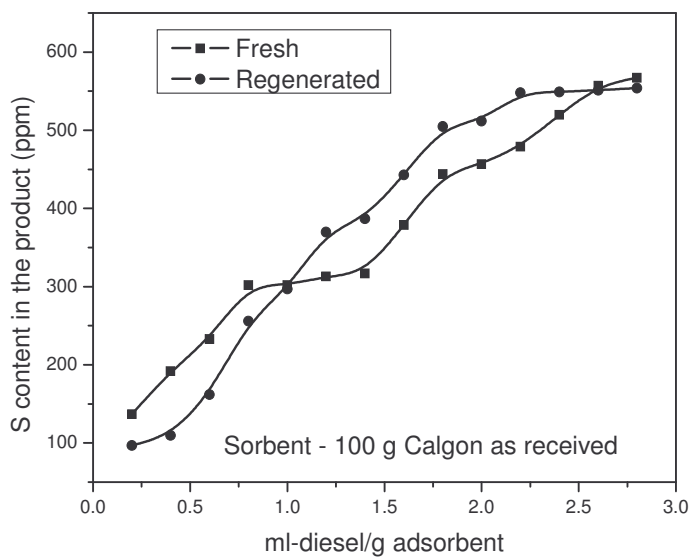


Fig. 28. Plot of S removal capacity of fresh Vs toluene regenerated sorbent (100 g calgon carbon as received)

An efficient desulphurization process based on adsorption, operated under modest conditions of temperature and pressure is developed. The potential of the process of adsorptive desulphurization lies in the elimination of refractive S containing compounds under mild process parameters. New method of activation, which is a unique combination of nitric acid treatment and Ar activation, of carbon based adsorbents to induced desired surface functionality, polarity, phase structure and pore texture, is developed. It was found that subsequent Ar activation of nitric acid treated carbon adsorbents is inevitable to derive the best out of oxidative modification of carbon surface chemistry. The utility of Adsorbent carbon as well as Calgon carbon and their tailored forms as adsorbents for organo sulphur compounds is nicely elucidated. The process of adsorptive desulphurization is scaled upto 100 g (adsorbent) batch. In addition to the successful removal of appreciable amounts of S from diesel feed stocks using tailored carbon based adsorbents, simple, inexpensive, efficient, environmentally benign and reliable solvent (toluene) based regeneration has also been developed. The study strengthened our hope that newer desulphurization technologies are not too far to the refinery industry.

V. CONCLUSION

The development of carbon materials has always been a challenging problem from the points of view of source of carbon materials, activation procedures that can be easily adopted and also exploiting them for various applications including as support for electrodes as well as for some specific catalytic applications. In this presentation, it has been demonstrated how the appropriate activation treatments can be developed keeping in mind the required textural characteristics. The possibility of employing these developed carbon materials or other carbon materials available from other sources in some applications as supports for electro-catalysts as well as using them for specific applications like adsorptive desulphurization has been considered.

IV. ACKNOWLEDGEMENTS

The authors wish to record their gratefulness to the Department of Science and Technology, India, for the support to the National Center for Catalysis Research. The authors are grateful to the authorities of The Chennai Petroleum Corporation Limited (CPCL) for sponsoring a research project at National Center for Catalysis Research (NCCR) on “Adsorptive Desulphurization of SR diesel from Cauvery Basin Refinery

Distillation Unit". Grateful thanks are also due to Ms. Columbian Chemicals Company, USA, for supporting the work.

V. REFERENCES:

- [1] B. Viswanathan, P. Indra Neel, T. K. Varadarajan, *Methods of Activation and Specific Applications of Carbon Materials*, E-book, February 2009, <http://nccr.iitm.ac.in>
- [2] B. Viswanathan and M. Aulice Scibioh, *Fuel Cells: Principles and Applications*, Universities Press, 2006
- [3] B. Ren, X. Q. Li, C. X. She, D. Y. Wu, Z. Q. Tian, *Electrochimica Acta* 46 (2000) 193
- [4] A. C. Sonia, Carabineiro and David T. Thompson, *Catalytic Applications of Gold Nanotechnology in Nanoscience and Technology*, Nanocatalysis, U. Heiz, U. Landman (Eds.), Springer-Verlag, Berlin Heidelberg, 2007, p. 463.
- [5] B. Rajesh, Ph. D., Thesis, Indian Institute of Technology Madras, 2002.
- [6] Andrew L. Dicks, *Journal of Power Sources*, 156 (2006) 128
- [7] Yicheng Liu, Xinpeng Qiu, Zhenguo Chen, Wentao Zhu, *Electrochemistry Communications* 4 (2002) 550
- [8] P. V. Samant, C. M. Rangel, M. H. Romero, J. B. Fernandes, J. L. Figueiredo, *Journal of Power Sources* 151 (2005) 79
- [9] J. L. Gomez de la Fuente, M. V. Martinez-Huerta, S. Rojas, P. Terreros, J. L. G. Fierro, M. A. Pena, *Catalysis Today* 116 (2006) 422
- [10] Gang Wu, Bo-Qing Xu, *Journal of Power Sources*, 174 (2007) 148
- [11] B. Viswanathan, *Catalysis Today*, 141 (2009) 52
- [12] Yupeng Guo, Shaofeng Yang, Kaifeng Yu, Jingzhe Zhao, Zichen Wang, Hongding Xu, *Materials Chemistry and Physics* 74 (2002) 320
- [13] Yong bin Ji, Tiehu Li, Li Xiaoxian Wang, Qilang Lin, *Applied Surface Science*, 254 (2007) 506.
- [14] P. Battistoni, S. Bompadre and G. Fava, *Materials Chemistry and Physics*, 11 (1984) 339
- [15] Joong S. Noh and James A. Schwarz, *Carbon* 28 (1990) 675
- [16] P. Vinke, M. Van Der Eijk, M. Verbree, A. F. Voskamp and H. Van Bekkum, *Carbon* 32 (1994) 675

- [17] A. Gil, G. Dela Puente, P. Grange, *Microporous Materials* 12 (1997) 51
- [18] V. Gomez-Serrano, M. Acedo-Ramos, A. J. Lopez-Peinado, C. Valenzuela-Calahorro, *Thermo Chimica Acta* 291 (1997) 109
- [19] Jae – Woon Shim, Soo – Jin Park, Seung – Kon Ryu, *Carbon* 39 (2001) 1635
- [20] Abdel-Nasser A. El-Hendaway, *Carbon* 41 (2003) 713f
- [21] Naiqin Zhao, Nawei, Jiajun Li, Zhijun Qiao, Jing Cui, Fei He, *Chemical Engineering Journal* 115 (2005) 133
- [22] E. M. Cuerda – Correa, M. Olivares – Marin, J. Ganan – Gomez, *Applied Surface Science*, 252 (2006) 5972
- [23] Mohindar S. Seehra and Arthur S. Pavlovic, *Carbon* 31 (1993) 557
- [24] V. Suresh Babu and M. S. Seehra, *Carbon* 34 (1996) 1259
- [25] Jean Baptiste Donnet, Roopchand Bansal, Meng-Jiao Wang, *Carbon Black – Science and Technology*, Second Edition, Revised and Expanded, CRC publications,
- [26] A. Manivannan, M. Chirila, N. C. Giles, M. S. Seehra, *Carbon* 37 (1999) 1741
- [27] A. R. West, *Solid State Chemistry and its Applications*, Wiley, Chichester, 1984, Pp. 734
- [28] Zhaolin Liu, Xing Yi Ling, Xiaodi Su and Jim Yang Lee, *J. Phys. Chem. B.*, 108 (2004) 8234
- [29] R. Manohara, J. B. Goodenough, *Journal of Materials Chemistry*, 2 (1992) 875
- [30] Zhaolin Liu, Jim Yang Lee, Weixiang Chen, Ming Han and Leong Ming Gan, *Langmuir* 20 (2004) 181
- [31] M. Sevilla, C. Sanches, T. Valdos-Sols, E. Moralln, A. B. Fuertes, *Journal of Physical Chemistry C*, 111 (2007) 9749
- [32] Jun Jie Niu, Jian Nong Wang, Li Zhang and Yiqing Shi, *Journal of Physical Chemistry C*, 111 (2007) 10329
- [33] Zhibin Lei, Shiyang Bai, Yi Xiao, Liqin Dang, Lizhen Au, Guangning Zhang, and Qian Xu, *Journal of Physical Chemistry C*, 111 (2008) 722
- [34] Shu-Fa Zheng, Jin-song Hu, Liang – Shu, Zhong, Li – Jun Wan, Wei-Guo Song, *Journal of Physical Chemistry C* 111 (2007) 11174
- [35] J. Sobkowski, K. Franaszczuk and K. Dobrowolska, *Journal of Electroanalytical Chemistry*, 330 (1992) 529

- [36] Zhaolin Liu, Jim Yang Lee, Weixiang Chen, Ming Han and Leong Ming Gan, *Langmuir* 20 (2004) 181
- [37]. Meng-Liang Lin, Chun-Chieh Huang, Man-Yin Lo, and Chung-Yuan Mou, *Journal of Physical Chemistry C*, 112 (2008) 867
- [38] Zhibin Lei, Lizhen An, Liquin Dang, Mingyi Zhao, Jingying Shi, Shiyong Bai, yindicao, *Microporous and Mesoporous Materials* 119 (2009) 301
- [39] H. J. Wang, H. Yu, F. Peng, P. Lv, *Electrochemistry communications* 8 (2006) 499
- [40] Maria Jasienko – Halat, Katarzyna Kedzior, *Carbon* 43 (2005) 944
- [41] Kiyoshi Okada, Nohuo Yamamoto, Yoshikazu Kameshima and Atsuo Yasumori, *Journal of Colloid and Interface Science* 262 (2003) 179
- [42] Ru-Ling Tseng, *Journal of Hazardous Materials* 147 (2007) 1020
- [43] B.Viswanathan, T. K. Varadarajan, P. Indra Neel, A process for the preparation of activated carbon from botanical sources, *Indian Pat. Appl.* (2008), IN 2007CH00376 A 20081128
- [44] Zhonghua Hu and E. F. Vansant, *Journal of Colloid and Interface Science*, 176 (1995) 422
- [45] F. Caturla, M. Molina-Sabio and F. Rodriguez-Reinoso, *Carbon* 29 (1991) 999
- [46] A. Ahmadpour and D. D. Do, *Carbon* 34 (1996) 471
- [47] K. Anoop Krishnan, *Colloids and Surfaces A: Physicochem. Eng. Aspects* 317 (2008) 344
- [48] Reynaldo Nacco and Eugenio Aquarone, *Carbon* 16 (1978) 31
- [49] J. de D. Lopez-Gonzalez, F. Martinez-Vilchez and F. Rodriguez-Reinoso, *Carbon* 18 (1980) 413
- [50]. Rafael Kandiyoti, John I Lazaridis, Bo Dyrvold and C. Ravindra Weerasinghe, *Fuel* 63 (1984) 1583
- [51] M. Z. Hussein, R. S. H. Tarmizi, Z. Zainal, R. Ibrahim and M. Badri, *Carbon* 34 (1996) 1447
- [52]. Jale Yanik, Mehmet Saglam, Guldem Ustun and Mithat Yuksel, *Fuel* 71 (1992) 712
- [53] C. Namasivayam and K. Kadirvelu, *Bioresource Technology* 62 (1997) 123
- [54]. Timothy G. Rials and Wolfgang G Glasser, *Journal of Applied Polymer Science* 37 (1989) 2399

- [55] Diana C. S. Azevedo, J. Cassia S. Araujo, Moises, Bastos-Neto, A. Eurico B. Torres, Emerson F Jaguaribe, Celio L. Cavalcante, *Microporous and Mesoporous Materials* 100 (1-3) (2007) 361
- [56] Mehmet Ugurlu, Ahmet Gurses Metin Acikyildiz, *Microporous and Mesoporous Materials* 111 (2008) 228
- [57] Devarly Prahas, Y. Kartika, N. Indraswati, S. Ismadji, *Chemical Engineering Journal*, 140 (2008) 32
- [58] Vilas Ganpat Pol, Menachem Motiei, Aharon Gedanken, Jose Calderon-Moreno, Masahiro Yoshimura, *Carbon* 42 (2004) 111
- [59] W. Ruland, *Advanced Materials*, 2 (1990) 528
- [60] W. Ruland, B. Smarsly, *Journal of Applied Crystallography*, 35 (2002) 624
- [61] Ting Yang, Aik Chong Lua, *Materials Chemistry and Physics*, 100 (2006) 438
- [62] M. Nakamizo, R. Kammereck and P. L. Walker, JR, *Carbon* 12 (1974) 259
- [63] Diane S. Knight and William B White, *Journal of Materials Research*, 4 (1989) 385
- [64] A. W. P. Fung, A. M. Rao, K. Kuriyama, M. S. Dresselhaus, G. Dresselhaus, M. Endo, N. Shindo, *Journal of Materials Research*, 8 (1993) 498
- [65] A. M. Rao, A. W. P. Feng, M. S. Dresselhaus, M. Endo, *Journal of Materials Research*, 7 (1992) 1788
- [66] X. K. Li, L. Liu, Zh. H. Li, D. Wu, Sh. D. Shen, *Carbon* 38 (2000) 623
- [67] M. Nakamizo and H. Honda and M. Inagaki and Y. Hishiyama, *Carbon* 15 (1977) 295
- [68] M. Nakamizo, H. Honda and M. Inagaki, *Carbon* 16 (1978) 281
- [69] Y. Sato, M. Kamo and N. Setaka, *Carbon* 16 (1978) 279
- [70] Terrence P. Mernagh, Ralph P. Cooney and Robert A. Johnson, *Carbon* 22 (1984) 39
- [71] B. H. Hameed, A. T. M. Din, A. L. Ahmed, *Journal of Hazardous Materials* 141 (2007) 819
- [72] Hee Jin Jeong, Seung Yol Jeong, Young Min Shin, Jeong Ho Han, Seong Chu Lim, Sung Jin Eum, Cheol woong Yang, Nam-gyun Kim, Chong – Yum Park, Young Hee Lee, *Chemical Physics Letters* 361 (2002) 189
- [73] Jieshan Qiu, Yongfeng Li, Yunpeng Wang, Changhai Liang, Tonghua Wang, Dehe Wang, *Carbon* 41 (2003) 767

- [74] P. Lespade, R. Al-Jishi and M. S. Dresselhaus, *Carbon* 20 (1982) 427
- [75] F. A. Cotton, G. Wilkinson, *Basic Inorganic Chemistry*, John Wiley & Sons, 1976.
- [76]. Sanjay Sarkar, Basudam Adhikari, *European Polymer Journal* 37 (2001) 1391
- [77]. D M Makay and P V Roberts 20 (1982) 87
- [78] Satoshi Kubo, Yasumitsu Uraki and Yoshihiro Sano, *Journal of Wood Science*, 49 (2003) 188
- [79] Viboon Sricharoenchaikul, Chiravoot Pechyen, Duangdao Aht-ong, and Duangduen Atong, *Energy and Fuels*, 22 (2008) 31
- [80] Stephen Brunauer, Lola S Deming, W. Edwards, Deming, Edward Teller, 62 (1940) 1723
- [81]. Wei Li, Li-bo Zhang, Jin – hui Peng, Ning Li, Xue – yun Zhu, *Industrial Crops and Products* 27 (2008) 341
- [82] S. J. Greg and K. S. W. Sing, *Adsorption, Surface Area and Porosity*, Second Edition, New York, Academic Press, 1982.
- [83] Y. Chen, J. Chen, H. Hu, M. A. Hamon, M. E. Itkis and R. C. Haddon, *Chemical Physics Letters* 299 (1999) 532
- [84] S. Mrozowski, *Carbon* 17 (3) (1979) 227
- [85]. R Sarathi, P Rajesh Kumar, R. H. Sahu, *Polymer Degradation and Stability* 92 (2007) 560
- [86] L. S. Singer and G. Wagoner, *Carbon* 6 (1968) 199
- [87] O. Chauvert, L. Forro, *Physical Review B (Condensed Matter and Materials Physics)*, 52 (1995) R6963
- [88] O. Zhuo, R. M. Fleming, D. W., Murphy, C. H. Chen, R. C. Haddon, A. P. Ramirez, S. H. Gharum, *Science* 263 (1994) 1744
- [89] Jair C. C. Freitas, Tito J. Bonagamba, Francisco G Emmerich, *Carbon* 39 (2001) 535
- [90] M. D. Adams, *Hydrometallurgy*, 26 (1991) 201
- [91] Francesco Ancillotti, Vittorio Fattore, *Fuel Processing Technology* 57 (1998) 163
- [92] Nezahat Boz, Timur Dogu, Kirali Murtezaoglu, Gulsen Dogu, *Catalysis Today* 100
- [93] Zeynep Obali, Timur Dogu, *Chemical Engineering Journal*, 138 (2008) 548
- [94] Ganapati D Yadav and Ambareesh D Murkute, *J. Phys. Chem. A.*, 108 (2004) 9557

- [95] S. J. Sardhar Basha, P. Vijayan, K. Santhi, D. K. Setua, *Catalysis Communications* 8 (2007) 619
- [96] John R Anderson and Michel Boudart, *Catalysis Science and Technology*, Volume 11, Springer Verlag, 1996
- [98] Frances M. Collins, Andrew R. Lucy, Christopher Sharp, *Journal of Molecular Catalysis A: Chemical*, 117 (1997) 397
- [99] Beatriz Castro, Michael J. Whitecombe, Evgeny N. Vulfson, Rafael Vazquez – Duhalt, Eduardo Barzana, *Analytica Chimica Acta*, 435 (2001) 83
- [100] Chunshan Song, Xiaoliang Ma, *Applied Catalysis B: Environmental*, 41 (2003) 207
- [101] Hai Mei, B. W. Mei, Teh Fu Yen, *Fuel* 82 (2003) 405
- [102] Chunshan Song, *Catalysis Today* 86 (2003) 211
- [103] Jorge Aburto, Antonio Mendez – Orozco, Sylvie Le Borgne, *Chemical Engineering and Processing*, 43 (2004) 1587
- [104] Yosuke Sano, Ki-Hyonk Choi, Yozo Korai, Isao Mochida, *Applied Catalysis B : Environmental* 49 (2004) 219
- [105] Xiaoliang Ma, Subramani Velu, Jae Hyung Kim, Chunshan song, *Applied Catalysis B: Environmental* 56 (2005) 137
- [106] Chang Yu, Jie Shan Qiu, Yu Feng Sun, Xian Hui Li, Gang Chen, Zong Bin Zhao, *Journal of Porous Materials* 15 (2008) 151
- [107] Yahia A. Alhamed, Hisham S. Bamufleh, *Fuel* 88 (2009) 87
- [108] I. V. Babich, J. A. Moulijn, *Fuel* 82 (2003) 607
- [109] Mohammad Farhat Ali, Abdullah Al-Malki, Massam El-Ali, Gary Martinie, Mohammad N. Siddiqui, *Fuel* 85 (2006) 1354
- [110] Chawalit Ngamcharussrivichai, Chatchawan Chatratanonon, Sakdinun Nuntang, Pattarapan Prasassarakich, *Fuel* 87 (2008) 2347
- [111] V. Selvavathi, V. Chidambaram, A. Meenakshisundaram, B. Sairam, B. Sivasankar, *Catalysis Today* 141 (2009) 99
- [112] Z. Y. Zhang, T. B. Shi, C. Z. Jia, W. J. Ji, Y. Chen, M. Y. He, *Applied Catalysis B: Environmental* 82 (2008) 1
- [113] Eri Ito, J. A. Rob Van Veen, *Catalysis Today* 116 (2006) 446

- [114] V. Selvavathi, A. Meenakshisundaram, B. Sairam, P. Indra Neel, M. Rajasekaran, B. Viswanathan, Adsorptive desulphurization of diesel by modified carbons, 6th International Symposium on Fuels and Lubricants (ISFL-2008)”, March 9-12, 2008 at New Delhi.
- [115] Joong S. Noh and James A. Schwarz, Carbon 28 (1990) 675
- [116] V. Gomez-Serrano, M. Acedo-Ramos, A. J. Lopez-Peinado, C. Valenzuela-Calahorro, Thermo Chimica Acta 291 (1997) 109
- [117] Mingwang Shao, Debao Wang, Guihua-Yu, Bing Hu, Weichao Yu, Yitai Qian, Carbon 42 (2004) 183-185.
- [118] J. A. Macia – Agullo, B. C. Moore, D. Cazorla – Amoros, A. Linares – Solana, Microporous Materials 101 (2007) 397
- [119] Qingrong Qian, Motoi Machida, Hideki Tatsumoto, Bioresource Technology, 98 (2007) 353-360
- [120] Thio Christine Chandra, M. M. Mirna, Y. Sudaryanto, S. Ismadji, Chemical Engineering Journal, 127 (2007) 121
- [121] A. M. Puziy, O. I. Poddubnaya, A. Martinez – Alonso, F. Suarez – Garcia, J. M. D. Tascon, Carbon 41 (2003) 1181
- [122] T. Budinova, E. Ekinci, F. Yardim, A. Grimm, E. Bjornbom, V. Minkova, M. Goranova, Fuel Processing Technology 87 (2006) 899
- [123] C. Ishizaki and I Marti, Carbon, 19 (1981) 409
- [124] M. Madhava Rao, A. Ramesh, G. Purna Chandra Rao, K. Sessaiah, Journal of Hazardous Materials B129 (2006) 123
- [125] Alexander M. Puziy, Olga I Poddubnaya, Amelia Martinez – Alonso, Fabian Suarez – Garcia, Jaun M. D. Tascon, Carbon 43 (2005) 2857
- [126] Ozgul Gercel, Adnan Ozcan, A. Safa Ozcan, H. Ferdi Gercel, Applied Surface Science, 253 (2007) 4843
- [127] A. Macias – Garcia, M. A. Diaz – Diez, E. M. Cuerda – Correa, M. Olivares – Marin, J. Ganan – Gomez, Applied Surface Science 252 (2006) 5972